Optimal Collaborative Mapping of Terrestrial Transmitters: Receiver Placement and Performance Characterization

JOSHUA J. MORALES, Student Member, IEEE
ZAHER M. KASSAS, Senior Member, IEEE
University of California, Riverside, Riverside, CA USA

Mapping multiple unknown terrestrial signals of opportunity (SOP) transmitters via multiple collaborating receivers is considered. The receivers are assumed to have knowledge about their own states, make pseudorange observations on multiple unknown SOPs, and fuse these pseudoranges through a central estimator. Two problems are considered. The first problem assumes multiple receivers with random initial states to pre-exist in the environment. The question of where to optimally place an additional receiver so to maximize the quality of the estimate of the SOPs' states is addressed. A novel, computationally efficient optimization criterion that is based on area-maximization is proposed. It is shown that the proposed optimization criterion yields a convex program, the solution of which is comparable to two classical criteria: minimization of the geometric dilution of precision (GDOP) and maximization of the determinant of the inverse of the GDOP matrix. The second problem addresses the optimal mapping performance as a function of time and number of receivers in the environment. It is demonstrated that such optimal performance assessment could be generated off-line without knowledge of the receivers' trajectories or the receivers' estimates of the SOP. Experimental results are presented demonstrating collaborative mapping of an unknown terrestrial SOP emanating from a cellular tower for various receiver trajectories versus the optimal mapping performance.

Manuscript received September 10, 2016; revised May 6, 2017, July 28, 2017, and October 4, 2017; released for publication October 9, 2017. Date of publication November 13, 2017; date of current version April 11, 2018.

DOI. No. 10.1109/TAES.2017.2773238

Refereeing of this contribution was handled by G. X. Gao.

This work was supported in part by the Office of Naval Research under Grant N00014-16-1-2305.

Authors' address: J. J. Morales and Z. M. Kassas are with the Department of Electrical and Computer Engineering, University of California, Riverside, Riverside, CA 92521 USA, E-mail: (jmora047@ucr.edu; zkassas@ieee.org). *(Corresponding author: Zaher M. Kassas.)*

I. INTRODUCTION

Optimal mapping is an important objective that arises in many application domains, such as source localization [1], target tracking [2], and autonomous vehicle navigation [3]. The mapping problem can be abstracted to that of estimating desired states in the environment, given information extracted from a sensor or a sensor network. Map optimality is furnished by considering a desired performance criterion, such as minimization of uncertainty, convergence time, and computational time.

While increasing the number of mapping sensors typically improves the quality of the produced maps, introducing additional sensors may be prohibitive due to economical, physical, or computational constraints. Optimal sensor placement has been studied as an enabling tool to achieve optimal mapping by using only a subset of available sensors for source localization [4], [5] and target tracking [6]–[9]. In autonomous vehicle navigation, environmental features are mapped *a priori* or on-the-fly, and these maps are used to estimate the vehicle's motion within the environment. These features could posses 1) a static state space, such as stationary landmarks (e.g., traffic lights, poles, buildings, etc.) or 2) a dynamic state space, such as transmitters of radio signals of opportunity (SOPs), which are not intended for positioning, navigation, or timing (e.g., AM/FM radio, cellular, and television signals). This paper considers the problem of optimal collaborative mapping of unknown terrestrial SOPs. This problem is important in two contexts: 1) unknown emitter localization and 2) opportunistic navigation.

Opportunistic navigation aims to exploit ambient radio frequency SOPs in the environment to improve navigation robustness and accuracy in global navigation satellite system (GNSS)-challenged environments [10]–[13]. Opportunistic navigation treats all ambient radio frequency signals as sources of information for navigation, such as AM/FM radio [14], cellular [15], [16], television [17], Iridium [18], and Wi-Fi [19]. SOPs are abundant, powerful, and available at various frequencies and geometric configurations, making them an attractive stand-alone navigation system whenever GNSS signals become inaccessible or untrustworthy. Even when GNSS signals are available, SOP observables can be coupled with GNSS observables to significantly improve the accuracy of the navigation solution [20].

In contrast to GNSS signals, SOPs are not intended for navigation. In particular, while information about GNSS space vehicle (SV) states are readily accessible, the states of SOPs may not be known *a priori*. Therefore, a first step in exploiting SOPs is to map their states. This can be accomplished either in 1) a mapping framework in which receivers have knowledge of their own states (by having access to GNSS signals, for example) [21] or 2) a simultaneous localization and mapping framework in which the receivers' states are simultaneously estimated with the SOPs' states [22].

Collaboration generally improves navigation. In collaborative opportunistic navigation, multiple receivers share their observations of SOPs in the environment to construct and continuously refine a global signal landscape map. Such signal landscape could be cloud-hosted, such that whenever GNSS signals become inaccessible or untrustworthy, the receivers continue navigating with the aid of this map [23]. The quality of the constructed map depends on the quality of the observations and the spatial geometry between the SOPs and receivers. The quality of the constructed map could be improved by prescribing the receivers' motion to minimize the uncertainty about the SOPs' together with the receivers' states assuming the initial states of all receivers to be unknown [24]. This motion planning could be generated in a greedy [25] or a receding horizon fashion [26].

This paper considers the following two problems. The first problem assumes that multiple receivers with random initial states are dropped in a planar environment comprising multiple unknown terrestrial SOPs with a random configuration. Each receiver has *a priori* knowledge about its own states (e.g., from GNSS observables). The receivers draw pseudorange observations from each SOP, which are fused through a centralized estimator that estimates the states of all SOPs. It is desired to reduce the uncertainty of the produced state estimates. However, in many practical scenarios, the receivers may be prevented from moving to more favorable locations to achieve the best reduction in uncertainty, e.g., if their motion is constrained or moving to new locations would consume a considerable amount of time or energy. Instead, it may be more efficient to deploy an additional collaborating receiver. Where should this additional receiver be placed to minimize the uncertainty about the SOPs' states?

The second problem considers a planar environment comprising N *mobile* receivers with knowledge about their own states, making pseudorange observations on *one* unknown terrestrial SOP, and fusing their observations through a centralized estimator. What is the optimal mapping performance as a function of time and N? The answer to this question would enable one to determine the minimum number of receivers that must be deployed in an environment to achieve a desired estimation uncertainty within a specified period of time.

Similar questions to the first problem this paper considers have arisen in other contexts, such as optimal GNSS SV distribution and selection [27]–[30] and optimal sensor placement for target localization and tracking [9], [31], [32]. Common metrics to assess the quality of the spatial geometry of GNSS SVs and range-based sensors are the geometric dilution of precision (GDOP) [33] and the determinant of the inverse of the GDOP matrix [27]. The GDOP is related to the sum of the variances of a position estimate. Therefore, smaller GDOP values (or larger determinants of the inverse of the GDOP matrix) correspond to more favorable geometries for localization. It was demonstrated in [28] that the GDOP at the center of an N-sided polygon is minimized when the sensors' locations form the vertices of a regular polygon. In [34], this sensor configuration was also shown to achieve the upper bound of the determinant of the Fisher information matrix (FIM), which is proportional to the inverse of the GDOP matrix. In [35], the area of a polygon inscribed in the unit circle whose vertices are the line of sight (LOS) vectors from the receiver (target) to the SVs (sensors) was presented as an alternative optimization function for selecting the best SVs.

While previous work considered optimizing the location of a constellation of SVs or a group of sensors with respect to a specified criterion, this paper assumes that N of the receivers are *arbitrarily* placed, and treats the problem of optimal placement of an *additional* $(N+1)$st receiver to improve the estimate of the SOPs' states. This introduces two main challenges when compared to optimizing the location of *all* available sensors. First, the optimal placement of the $(N+1)$st sensor is dependent on the distribution of the pre-deployed sensors, whereas the optimal placement of all available sensors is only dependent on the number of sensors whose optimal configuration is a regular polygon. Second, the optimal placement of the $(N+1)$st sensor is dependent on the optimization criterion employed, whereas the optimal placement of all available sensors is invariant to the optimization criterion (GDOP minimization, determinant of the inverse of the GDOP matrix maximization, and area maximization).

A preliminary study comparing the problems of GDOP minimization, determinant of the inverse of the GDOP matrix maximization, and area maximization, for optimal placement of an additional $(N+1)$st receiver was conducted in [36]. It was demonstrated that these three optimization problems are comparable and that the area maximization problem is piecewise-concave with a simple analytical solution. However, only an environment comprising a *single* SOP was considered. Optimal sensor placement for multiple target positioning was considered in [37] by maximizing the determinant of the FIM. However, the optimization was performed over the entire set of sensors.

This paper makes two contributions. First, the optimal receiver placement problem is extended to environments comprising *multiple* SOPs. To this end, a novel optimization criterion, namely, the product of areas maximization is derived. This optimization criterion is intimately related to the classical GDOP minimization and determinant of the inverse of the GDOP matrix maximization criteria, making it a good alternative for optimal receiver placement. The proposed optimization criterion yields a family of parallelizable convex programs and is computationally cheaper compared to the classical optimization criteria, which do not yield convex programs. Second, the optimal mapping performance in an environment comprising N mobile receivers estimating the states of one unknown terrestrial SOP is characterized as a function of time and N. The optimal mapping performance was originally demonstrated in [36], but was offered without a proof or an experimental demonstration. This paper presents a rigourous proof for the optimal mapping performance together with simulation and experimental results illustrating various receiver trajectories versus the optimal mapping performance. The

experimental results demonstrate collaborative mapping of an unknown cellular code division multiple access (CDMA) SOP transmitter to an unprecedented degree of accuracy. It is important to note that while this paper focuses on mapping SOPs for opportunistic navigation purposes, the developed techniques are widely applicable to other application domains involving range-type sensors.

The remainder of this paper is organized as follows. Section II describes the SOPs' dynamics and receivers' observation model. Section III formulates the optimal receiver placement problem for an arbitrary number of SOPs in the environment as GDOP minimization and determinant of the inverse of the GDOP matrix maximization. The placement problem is reformulated as an area maximization for the single SOP case and a product of areas maximization for the multiple SOP case. The area and product of areas optimization problems are compared against the GDOP optimization problems and their optimal solution is specified. Section IV derives the optimal mapping performance as a function of time and number of receivers. Section V presents experimental results for collaboratively mapping an unknown SOP. Concluding remarks are given in Section VI.

II. MODEL DESCRIPTION

The following nomenclature and conventions will be used throughout this paper. Vectors will be column and represented by lower-case, italicized, and bold characters, e.g., $\boldsymbol{x}$. Matrices will be represented by upper-case bold characters, e.g., $\mathbf{A}$.

A. SOP Dynamics Model

The SOP clock error dynamics will be modeled according to the two-state model composed of the clock bias δt_s and clock drift $\dot{\delta t}_s$. The clock error states $\boldsymbol{x}_{\text{clk},s}$ evolve according to

$$\dot{\boldsymbol{x}}_{\text{clk},s}(t) = \mathbf{A}_{\text{clk}}\,\boldsymbol{x}_{\text{clk},s}(t) + \tilde{\boldsymbol{w}}_{\text{clk},s}(t),$$

$$\boldsymbol{x}_{\text{clk},s} = \begin{bmatrix} \delta t_s \\ \dot{\delta t}_s \end{bmatrix}, \quad \tilde{\boldsymbol{w}}_{\text{clk},s} = \begin{bmatrix} \tilde{w}_{\delta t_s} \\ \tilde{w}_{\dot{\delta t}_s} \end{bmatrix}, \quad \mathbf{A}_{\text{clk}} = \begin{bmatrix} 0 & 1 \\ 0 & 0 \end{bmatrix},$$

where the elements of $\tilde{\boldsymbol{w}}_{\text{clk},s}$ are modeled as zero-mean, mutually independent white noise sequences, and the power spectral density of $\tilde{\boldsymbol{w}}_{\text{clk},s}$ is given by $\tilde{\mathbf{Q}}_{\text{clk},s} = \text{diag}\,[S_{\tilde{w}_{\delta t_s}}, S_{\tilde{w}_{\dot{\delta t}_s}}]$, where $\text{diag}[a, b]$ is an appropriately sized square matrix with diagonal elements a and b and zeros elsewhere. The power spectra $S_{\tilde{w}_{\delta t_s}}$ and $S_{\tilde{w}_{\dot{\delta t}_s}}$ can be related to the power-law coefficients $\{h_\alpha\}_{\alpha=-2}^{2}$, which have been shown through laboratory experiments to be adequate to characterize the power spectral density of the fractional frequency deviation $y(t)$ of an oscillator from nominal frequency, which takes the form $S_y(f) = \sum_{\alpha=-2}^{2} h_\alpha f^\alpha$ [38]. It is common to approximate the clock error dynamics by considering only the frequency random walk coefficient h_{-2} and the white frequency coefficient h_0, which lead to $S_{\tilde{w}_{\delta t_s}} \approx \frac{h_0}{2}$ and $S_{\tilde{w}_{\dot{\delta t}_s}} \approx 2\pi^2 h_{-2}$ [39].

The SOP will be assumed to emanate from a spatially-stationary terrestrial transmitter, and its state vector will consist of its planar position states $\boldsymbol{r}_s \triangleq [x_s, y_s]^{\mathsf{T}}$ and $c\,\boldsymbol{x}_{\text{clk},s}$, where c is the speed of light. Hence, the SOP's dynamics can be described by the state space model

$$\dot{\boldsymbol{x}}_s(t) = \mathbf{A}_s\,\boldsymbol{x}_s(t) + \mathbf{D}_s\,\tilde{\boldsymbol{w}}_s(t) \tag{1}$$

where $\boldsymbol{x}_s \triangleq [\boldsymbol{r}_s^{\mathsf{T}}, c\,\boldsymbol{x}_{\text{clk},s}^{\mathsf{T}}]^{\mathsf{T}}$, $\tilde{\boldsymbol{w}}_s \triangleq \tilde{\boldsymbol{w}}_{\text{clk},s}$

$$\mathbf{A}_s = \begin{bmatrix} \mathbf{0}_{2\times2} & \mathbf{0}_{2\times2} \\ \mathbf{0}_{2\times2} & \mathbf{A}_{\text{clk}} \end{bmatrix}, \quad \mathbf{D}_s = \begin{bmatrix} \mathbf{0}_{2\times2} \\ \mathbf{I}_{2\times2} \end{bmatrix}.$$

Discretizing the SOP's dynamics (1) at a constant sampling interval T yields the discrete-time (DT)-equivalent model

$$\boldsymbol{x}_s(k+1) = \mathbf{F}_s\,\boldsymbol{x}_s(k) + \boldsymbol{w}_s(k), \quad k = 1, 2, \ldots, \tag{2}$$

where $\boldsymbol{w}_s \triangleq \left[w_{x_s}, w_{y_s}, w_{\delta t_s}, w_{\dot{\delta t}_s}\right]^{\mathsf{T}}$ is a zero-mean white noise sequence with covariance $\mathbf{Q}_s$, and

$$\mathbf{F}_s = \text{diag}\,[\mathbf{I}_{2\times2}, \mathbf{F}_{\text{clk}}], \quad \mathbf{Q}_s = \text{diag}\left[\mathbf{0}_{2\times2}, c^2\mathbf{Q}_{\text{clk},s}\right],$$

$$\mathbf{F}_{\text{clk}} = \begin{bmatrix} 1 & T \\ 0 & 1 \end{bmatrix}, \; \mathbf{Q}_{\text{clk},s} = \begin{bmatrix} S_{\tilde{w}_{\delta t_s}} T + S_{\tilde{w}_{\dot{\delta t}_s}} \frac{T^3}{3} & S_{\tilde{w}_{\dot{\delta t}_s}} \frac{T^2}{2} \\ S_{\tilde{w}_{\dot{\delta t}_s}} \frac{T^2}{2} & S_{\tilde{w}_{\dot{\delta t}_s}} T \end{bmatrix}.$$

B. Observation Model

The pseudorange observation made by the nth receiver on the SOP, after discretization and mild approximations discussed in [22], is related to the SOP's states by

$$z_n(k) = \|\boldsymbol{r}_{r_n}(k) - \boldsymbol{r}_s\| + c\cdot\left[\delta t_{r_n}(k) - \delta t_s(k)\right] + v_n(k) \tag{3}$$

where $\|\cdot\|$ is the Euclidean norm, $\boldsymbol{r}_{r_n} \triangleq [x_{r_n}, y_{r_n}]^{\mathsf{T}}$ and δt_{r_n} are the position and clock bias of the receiver, respectively, and v_n is the measurement noise, which is modeled as a DT zero-mean white Gaussian sequence with variance σ_n^2.

III. OPTIMAL RECEIVER PLACEMENT

This section answers the question: where to optimally place a receiver in an environment comprising N randomly pre-deployed receivers and M unknown SOPs with an arbitrary configuration? The following section will formulate and compare three optimization problems: GDOP minimization, determinant maximization, and area maximization. Subsequently, the convexity of these problems is analyzed. Finally, an analytical solution to the area maximization problem is derived for two cases: single ($M = 1$) and multiple ($M > 1$) SOPs.

A. Problem Formulation

Consider a planar environment comprising M unknown SOPs and N arbitrarily placed receivers with knowledge about their own states. The receivers draw pseudorange observations from each SOP, denoted $\{{}^m z_n\}_{n=1}^{N}$, for $m = 1, \ldots, M$. These observations are fused through a centralized estimator whose role is to estimate the augmented state vector $\boldsymbol{x}'$ defined as

$$\boldsymbol{x}' \triangleq \left[\boldsymbol{x}_{s_1}'^{\mathsf{T}}, \ldots, \boldsymbol{x}_{s_M}'^{\mathsf{T}}\right]^{\mathsf{T}}, \quad \boldsymbol{x}_{s_m}' \triangleq \left[\boldsymbol{r}_{s_m}^{\mathsf{T}}, c\delta t_{s_m}\right]^{\mathsf{T}}.$$

It is desired to deploy an additional receiver to a location that will result in the maximum improvement of the estimate of $\boldsymbol{x}'$, denoted as $\hat{\boldsymbol{x}}'$. The measurement residual computed by the centralized estimator has a first-order approximation of its Taylor series expansion about $\hat{\boldsymbol{x}}'$, which is given by

$$\Delta \boldsymbol{z} = \mathbf{H}' \, \Delta \boldsymbol{x}' + \boldsymbol{v}, \tag{4}$$

where $\Delta \boldsymbol{z} \triangleq \boldsymbol{z} - \hat{\boldsymbol{z}}$, i.e., the difference between the observation vector

$$\boldsymbol{z} \triangleq \left[{}^1z_1, \ldots, {}^1z_{N+1}, {}^2z_1, \ldots, {}^2z_{N+1}, \ldots, {}^Mz_{N+1} \right]^{\mathrm{T}}$$

and its estimate $\hat{\boldsymbol{z}}$; $\Delta \boldsymbol{x}' \triangleq \boldsymbol{x}' - \hat{\boldsymbol{x}}'$, i.e., the difference between $\boldsymbol{x}'$ and its estimate $\hat{\boldsymbol{x}}'$; $\boldsymbol{v} \triangleq [{}^1\boldsymbol{v}^{\mathrm{T}}, \ldots, {}^M\boldsymbol{v}^{\mathrm{T}}]^{\mathrm{T}}$, where ${}^m\boldsymbol{v} \triangleq [{}^mv_1, \ldots, {}^mv_{N+1}]^{\mathrm{T}}$; and $\mathbf{H}'$ is the Jacobian matrix evaluated at the estimate $\hat{\boldsymbol{x}}'$, which is given by $\mathbf{H}' = \mathrm{diag}[\mathbf{H}'_1, \ldots, \mathbf{H}'_M]$, where

$$\mathbf{H}'_m = -\begin{bmatrix} {}^m\hat{\mathbf{l}}_1^{\mathrm{T}} & 1 \\ \vdots & \vdots \\ {}^m\hat{\mathbf{l}}_{N+1}^{\mathrm{T}} & 1 \end{bmatrix} = -\begin{bmatrix} \cos({}^m\phi_1) & \sin({}^m\phi_1) & 1 \\ \vdots & \vdots & \vdots \\ \cos({}^m\phi_{N+1}) & \sin({}^m\phi_{N+1}) & 1 \end{bmatrix}.$$

Without loss of generality, assume an East-North coordinate frame, denoted $\{f_m\}$, centered at the mth SOP's position estimate $\hat{\boldsymbol{r}}_{s_m}$. The vector ${}^m\hat{\mathbf{l}}_n \triangleq [\cos({}^m\phi_n), \sin({}^m\phi_n)]^{\mathrm{T}} = \frac{\boldsymbol{r}_{r_n} - \hat{\boldsymbol{r}}_{s_m}}{\|\boldsymbol{r}_{r_n} - \hat{\boldsymbol{r}}_{s_m}\|}$ is geometrically a unit LOS vector expressed in $\{f_m\}$ to the nth receiver position $\boldsymbol{r}_{r_n}$. The bearing angle ${}^m\phi_n$ will be measured counterclockwise with respect to the East axis of $\{f_m\}$ and $\boldsymbol{r}_{r_n}$ will be expressed in $\{f_1\}$. The observation noise for the set of measurements is assumed to be independent and identically-distributed (i.i.d.) across all channels, i.e., $\{\sigma_n^2\}_{n=1}^{N+1} \equiv \sigma^2$ and $\mathrm{cov}(\boldsymbol{v}) = \sigma^2 \mathbf{I}_{M(N+1)\times M(N+1)}$. The weighted least-squares solution to (4) and associated estimation error covariance $\mathbf{P}'$ are given by

$$\boldsymbol{\Delta}\hat{\boldsymbol{x}}' = \left(\mathbf{H}'^{\mathrm{T}}\mathbf{H}'\right)^{-1} \mathbf{H}'^{\mathrm{T}} \boldsymbol{\Delta}\boldsymbol{z}, \quad \mathbf{P}' = \sigma^2 \left(\mathbf{H}'^{\mathrm{T}}\mathbf{H}'\right)^{-1}. \tag{5}$$

The matrix $(\mathbf{H}'^{\mathrm{T}}\mathbf{H}')^{-1}$ is known as the GDOP matrix. Hence, the quality of the estimate depends on the receiver-to-SOP geometry and the pseudorange observation noise variance σ^2. The GDOP is defined as $\mathrm{GDOP} \triangleq \sqrt{\mathrm{tr}[(\mathbf{H}'^{\mathrm{T}}\mathbf{H}')^{-1}]}$, where $\mathrm{tr}[\cdot]$ is the matrix trace. The GDOP provides a simple scalar characterization of the receiver-to-SOP geometry–the lower the GDOP, the more favorable the geometry [33]. Therefore, the receiver placement problem can be cast as the GDOP minimization problem

$$\underset{\boldsymbol{r}_{r_{N+1}}}{\text{minimize}} \quad \sqrt{\mathrm{tr}\left[\left[\, \mathbf{H}'^{\mathrm{T}}(\boldsymbol{r}_{r_{N+1}})\mathbf{H}'(\boldsymbol{r}_{r_{N+1}}) \,\right]^{-1}\right]}, \tag{6}$$

where $\boldsymbol{r}_{r_{N+1}}$ is the location of the $(N+1)$st receiver. The GDOP is approximately minimized when the determinant $\det(\mathbf{H}'^{\mathrm{T}}\mathbf{H}')$ is maximized, since $(\mathbf{H}'^{\mathrm{T}}\mathbf{H}')^{-1} = \mathrm{adj}(\mathbf{H}'^{\mathrm{T}}\mathbf{H}')/\det(\mathbf{H}'^{\mathrm{T}}\mathbf{H}')$ and the adjoint $\mathrm{adj}(\mathbf{H}'^{\mathrm{T}}\mathbf{H}')$ varies less with the geometry of the receiver placement than $\det(\mathbf{H}'^{\mathrm{T}}\mathbf{H}')$ [33]. Therefore, an alternative optimization problem to (6) is

$$\underset{\boldsymbol{r}_{r_{N+1}}}{\text{maximize}} \quad \det\left[\, \mathbf{H}'^{\mathrm{T}}(\boldsymbol{r}_{r_{N+1}})\mathbf{H}'(\boldsymbol{r}_{r_{N+1}}) \,\right]. \tag{7}$$

The optimization problems (6) and (7) are equivalent to the so-called A- and D-optimality criteria, respectively [40]. In (6), the average variance of the estimates are minimized, whereas (7) is equivalent to minimizing the volume of the uncertainty ellipsoid, which has a useful geometric interpretation for receiver placement. This interpretation gives rise to an alternative optimization problem to both (6) and (7), which is formulated and compared in Sections III-B and III-C for $M = 1$ and $M > 1$, respectively.

B. Case One: Single SOP

For planar environments comprising a single SOP, (6) and (7) may be reparameterized over ${}^1\phi_{N+1}$, since $\mathbf{H}'$ is completely determined by the SOP-to-receiver bearing angles. Since the environment consists of only a single SOP, the superscript will be dropped to simplify notation for the remainder of this section, i.e., ${}^1\phi_n \equiv \phi_n$. It can be shown that $\det\left(\mathbf{H}'^{\mathrm{T}}\mathbf{H}'\right)$ is related to the area of the polytope inscribed in a unit circle, whose vertices are defined by the SOP-to-receiver unit LOS vector endpoints [27]. Hence, the optimization problem can be reformulated as a polytope area maximization problem over ϕ_{N+1}. In a planar scenario composed of three receivers, the relationship is exact, i.e., maximizing $\det\left(\mathbf{H}'^{\mathrm{T}}\mathbf{H}'\right)$ simultaneously maximizes the area of the triangle whose vertices are defined by the unit LOS vectors. This is due to the fact that $\mathbf{H}'$ is now a square matrix. With the exception of the scenario when all receivers are collinear with an SOP, $\mathbf{H}'$ is an invertible matrix and the area is $A = \frac{1}{2}\sqrt{\det(\mathbf{H}'^{\mathrm{T}}\mathbf{H}')} = \frac{1}{2}\det(\mathbf{H}')$. For more than three receivers, the relationship is exact for regular polygons, but approximate for non-regular polygons. Specifically, a polygon inscribed in the unit circle that simultaneously maximizes the determinant and maximizes the area is a regular polygon [35].

For non-regular polygons, the relationship is "almost exact" and the discrepancy is minimal. To see this, $N+1$ receivers were placed randomly around an SOP, where the nth receiver position was chosen such that $\phi_n \sim \mathcal{U}(0, 2\pi)$, for $n = 2, \ldots, N+1$, and $\phi_1 = 0$, for a total of 10^5 random configurations, where $\mathcal{U}(a, b)$ is the uniform distribution over (a, b). For each configuration, the corresponding GDOP and area were calculated, which are plotted in Fig. 1(a)–(d) for $N = 2, \ldots, 5$, respectively. Subsequently, for each of the configurations, the first N receivers' positions were fixed and the $(N+1)$st receiver was placed so to optimize the GDOP then to optimize the area. The resulting optimal GDOP versus optimal area are plotted in Fig. 1(e)–(h) for $N = 2, \ldots, 5$, respectively.

The following can be concluded from the plots in Fig. 1. First, placing the $(N+1)$st receiver to optimize the area simultaneously optimizes the GDOP only for $N = 2$. Second, for $N > 2$, placing the $(N+1)$st receiver to optimize the area approximately optimizes the GDOP. Third, the voids in the "point cloud" in the optimal area versus optimal

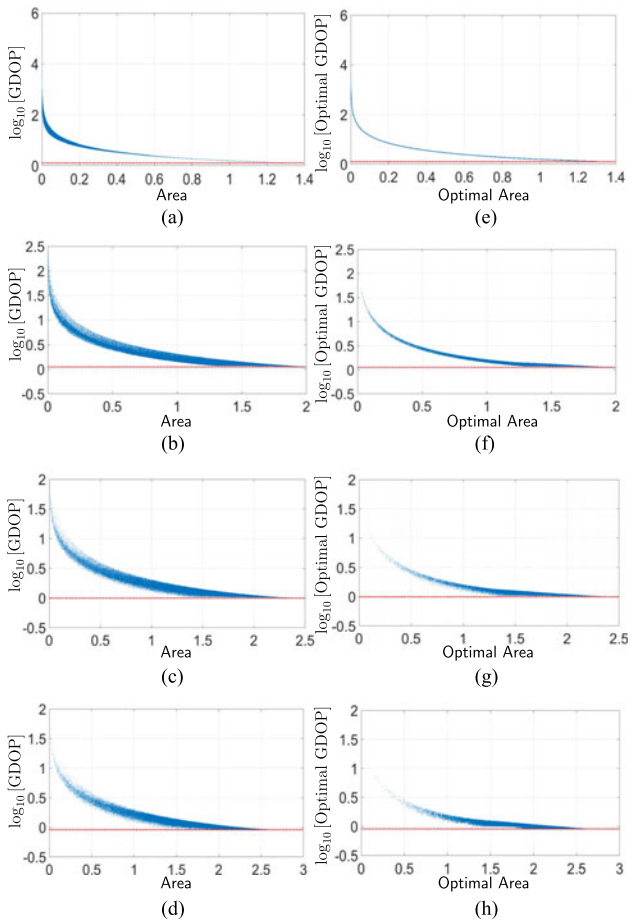

Fig. 1. $N+1$ receivers were randomly placed around an SOP for a total of 10^5 configurations. Fig. (a)–(d) correspond to $N = 2, \ldots, 5$, respectively, and Fig. (e)–(h) correspond to $N = 2, \ldots, 5$, respectively. For each configuration, the resulting area and the resulting GDOP were computed and plotted in Fig. (a)–(d). Each point in the point cloud represents the area and corresponding GDOP for a particular configuration. Then, for each previous configuration, the first N receiver locations were fixed and the $(N+1)$st receiver was optimally placed to optimize the GDOP and then to optimize the area. Each point in the point cloud plotted in Fig. (e)–(h) represents the optimal area versus optimal GDOP for a particular configuration. Dotted red line corresponds to the theoretical minimum achievable GDOP.

GDOP plot [see Fig. 1(e)–(h)] compared to the area versus GDOP plot [see Fig. 1(a)–(d)] are due to optimizing the placement of the $(N+1)$st receiver, which effectively increases the area (decreases the GDOP), pushing the "point cloud" towards the right (bottom). Fourth, when $N+1$ receivers are arranged so that the end-point's of the unit LOS vectors form a regular polygon configuration, the theoretical minimum GDOP, given by $\text{GDOP}_{\min} = \sqrt{5/(N+1)}$ is achieved (dotted red line in Fig. 1) [28] and the area simultaneously achieves its maximum value.

Motivated by these results, an alternative optimization problem to (6) and (7) is proposed, which aims to maximize the area A of the polygon over the angle of the unit LOS vector of the $(N+1)$st receiver, namely

$$\underset{\phi_{N+1}}{\text{maximize}} \quad A(\phi_{N+1}) = A_N + \Delta A(\phi_{N+1}), \tag{8}$$

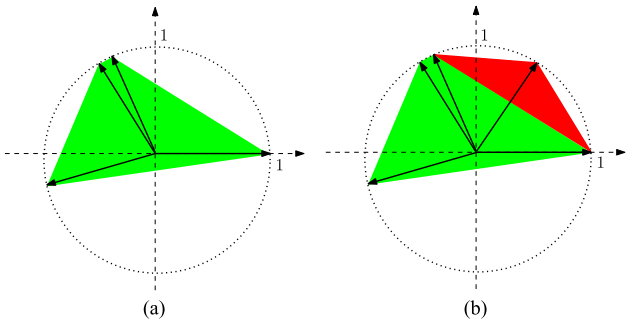

Fig. 2. (a) Polygon inscribed in the unit circle formed by the endpoints of the unit LOS vectors from the SOP to four randomly-deployed receivers for the configuration depicted in Fig. 3(a). The area A_N is highlighted in green. (b) Resulting polygon due to introducing an additional fifth receiver depicted in Fig. 3(a). The change in area $\Delta A(\phi_{N+1})$ due to introducing the $(N+1)$st receiver is highlighted in red.

where A_N is the total area for N pre-deployed receivers. The area A_N can be derived from the the sum of triangle areas as

$$A_N = \sum_{n=1}^{N} \frac{1}{2} \sin(\theta_n), \tag{9}$$

where $\theta_n \triangleq \phi_{n+1} - \phi_n$ for $n = 1, \ldots, N-1$; $\theta_N \triangleq 2\pi - \phi_N$; and $\Delta A(\phi_{N+1})$ is the change in area resulting from placing the $(N+1)$st receiver at ϕ_{N+1}, where $\phi_n \le \phi_{N+1} \le \phi_{n+1} < 2\pi$. The change in area $\Delta A(\phi_{N+1})$ is given by

$$\Delta A(\phi_{N+1}) = \frac{1}{2}\left[\sin(\phi_{N+1} - \phi_n) + \sin(\theta_n - \phi_{N+1} + \phi_n) - \sin(\theta_n)\right]. \tag{10}$$

A depiction of $A(\phi_{N+1})$ is illustrated in Fig. 2.

Next, it will be shown that while the optimization functions in (6) and (7) are neither convex nor concave, necessitating a general-purpose numerical nonlinear optimization solver, the optimization function in (8) is piecewise-concave with a simple analytical solution.

1) *Convexity Analysis:* The term $\mathbf{H}'^{\mathrm{T}}\mathbf{H}'$ in the optimization problems (6) and (7) can be readily shown to be

$$\mathbf{H}'^{\mathrm{T}}\mathbf{H}' = \sum_{n=1}^{N+1} \begin{bmatrix} \cos^2\phi_n & \cos\phi_n \sin\phi_n & \cos\phi_n \\ \sin\phi_n \cos\phi_n & \sin^2\phi_n & \sin\phi_n \\ \cos\phi_n & \sin\phi_n & 1 \end{bmatrix}.$$

It is obvious that the optimization functions in (6) and (7) are neither convex nor concave. However, while the optimization function (8) is neither convex nor concave, it is piecewise-concave, and the "zero-crossings" occur when the additional receiver is introduced at the same bearing angle as a pre-deployed receiver. A depiction of these functions is illustrated in Fig. 3.

2) *Optimal Solution to Area Maximization:* The special property of piecewise-concavity of the area maximization problem (8) allows for a simple analytical solution for the receiver placement problem. This is summarized in the following theorem.

THEOREM III.1 *The optimal placement with respect to the area maximization criterion (8) of a receiver to an*

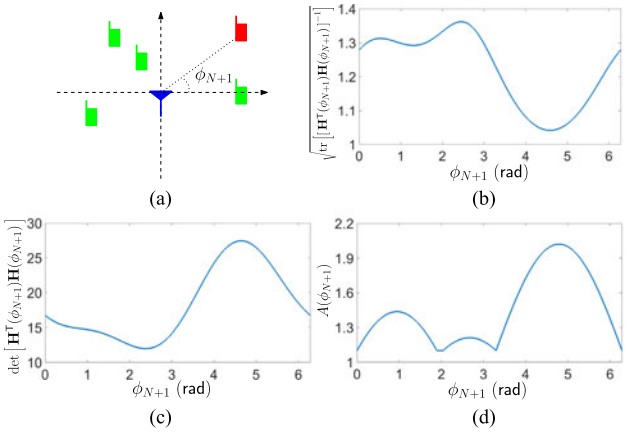

Fig. 3. (a) Four randomly placed receivers (green) with respective angles $\phi_n \in \{0, 1.892, 2.043, 3.295\}$ rad estimating the state vector of an unknown SOP (blue). The optimal receiver placement problem is to place an additional receiver (red) at an angle ϕ_{N+1} that will minimize the GDOP (6), maximize the determinant of the inverse of the GDOP matrix (7), or maximize the area of the polygon (8). The corresponding GDOP, determinant, and area optimization functions, respectively, due to sweeping $0 \le \phi_{N+1} \le 2\pi$ of the additional receiver, are plotted in (b)–(d).

environment comprising N arbitrarily placed receivers and one SOP is anywhere on a LOS vector from the SOP at an angle $\phi^{\star}_{N+1} = \frac{1}{2}\max_n \theta_n$, *for* $n = 1, \ldots, N$, *where* $\theta_n \triangleq \phi_{n+1} - \phi_n$, $n = 1, \ldots, N-1$ *and* $\theta_N \triangleq 2\pi - \phi_N$.

PROOF First, it will be shown that in a particular $\theta_n \in [0, 2\pi)$, the angle that maximizes the change in area is at $\phi^{\star(n)}_{N+1}$, where $\phi^{\star(n)}_{N+1} \triangleq \phi_n + \alpha^{\star}_n$ and $\alpha^{\star}_n = \frac{1}{2}\theta_n$, where α_n is defined as the angle sweeping θ_n, i.e., $\alpha_n \triangleq \phi_{N+1} - \phi_n$ for $0 \le \alpha_n \le \theta_n$.

Parameterizing $\Delta A(\phi_{N+1})$ by α_n in (10) yields

$$\Delta A(\alpha_n) = \frac{1}{2}\left[\sin(\alpha_n) + \sin(\theta_n - \alpha_n) - \sin(\theta_n)\right] \tag{11}$$

and applying the first-order necessary condition for optimality yields

$$\frac{d\Delta A(\alpha_n)}{d\alpha_n} = \frac{1}{2}\cos(\alpha_n) - \frac{1}{2}\cos(\theta_i - \alpha_n) \equiv 0$$
$$\Rightarrow \alpha^{\star}_n = \frac{1}{2}\theta_n + \pi k.$$

Substituting $\alpha^{\star}$ into the definition of $0 \le \alpha_n \le \theta_n$ yields $-\frac{1}{2}\theta_n \le \pi k \le \frac{1}{2}\theta_n$. Since the angle between any two known receivers is $0 \le \theta_n < 2\pi$, k is bounded by $-\pi < \pi k < \pi$. The only value of k that satisfies this inequality is $k = 0$. Therefore, $\alpha^{\star}_n = \frac{1}{2}\theta_n$ is the only critical angle in θ_n.

Furthermore, since $0 \le \theta_n < 2\pi$, the critical angle is $0 \le \alpha^{\star}_n < \pi$. The second-order necessary condition for optimality, evaluated at this critical angle is

$$\begin{aligned}\frac{d^2\Delta A_n}{d\alpha_n^2} &= -\frac{1}{2}\sin(\alpha_n) - \frac{1}{2}\sin(\theta_n - \alpha_n)\\ &= -\frac{1}{2}\sin(\alpha^{\star}_n) - \frac{1}{2}\sin(2\alpha^{*}_n - \alpha^{*}_n)\\ &= -\sin(\alpha^{\star}_n).\end{aligned} \tag{12}$$

Algorithm 1: Optimal Receiver Placement for One SOP.

Given: Positions of all pre-deployed receivers and an estimate of the SOP's position.
Calculate the angles $\{\theta_n\}_{n=1}^{N}$ sandwiched between every two consecutive receivers.
Halve the largest of these angles.
Place the $(N+1)$st receiver anywhere on a ray with the angle calculated in the previous step.

Since (12) is always negative, the change in area in (10) is concave over $\phi_n + \theta_n$, and $\alpha^{\star}$ is the global maximizer. The above analysis holds $\forall\theta_n$, and the change in area over $[0, 2\pi)$ is piecewise-concave with N concave regions, where each region corresponds to $\{\theta_n\}_{n=1}^{N}$.

Next, it will be shown that the largest change in area $\Delta A(\phi_{N+1})$ is achieved when the largest region θ_n is chosen, i.e., the receiver is positioned at $\phi^{\star}_{N+1} = \phi_{n_{\max}} + \alpha^{\star}_{n_{\max}}$, where $\phi_{n_{\max}} = \phi_{n_{\max+1}} - \theta_{n_{\max}}$, $\theta_{n_{\max}} \triangleq \max_n\{\theta_n\}$, $\alpha^{\star}_{n_{\max}} = \frac{1}{2}\theta_{n_{\max}}$, where $n = 1, \ldots, N$.

Substituting for $\alpha^{\star}_n = \frac{1}{2}\theta_n$ into (11) yields

$$\Delta A\left(\alpha^{\star}_n\right) = \sin\left(\frac{1}{2}\theta_n\right) - \frac{1}{2}\sin(\theta_n).$$

Taking the derivative with respect to θ_n yields

$$\frac{d\Delta A(\alpha_n)}{d\theta_n} = \frac{1}{2}\cos\left(\frac{1}{2}\theta_n\right) - \frac{1}{2}\cos(\theta_n). \tag{13}$$

Equation (13) is nonnegative from $[0, \frac{4\pi}{3}]$, i.e., increasing the region $\theta_n \in [0, \frac{4\pi}{3}]$ increases the resulting area. Hence, choosing $\theta_{n_{\max}}$ in this range guarantees the largest change in area. In $(\frac{4\pi}{3}, 2\pi)$, (13) is negative; therefore, the change in area begins to decrease as θ_n sweeps $(\frac{4\pi}{3}, 2\pi)$. To verify that choosing $\theta_{n_{\max}}$ is the optimal choice, it is shown that $\Delta A(\theta_n) < \Delta A(\theta_{n_{\max}})$, when $\theta_n \in [0, 2\pi - \Gamma]$, where $\Gamma = \theta_{n_{\max}} = \frac{4\pi}{3} + \varepsilon$, $0 < \varepsilon < \frac{2\pi}{3}$. Hence

$$\Delta A\left(\theta_{n_{\max}}\right) > \Delta A(\theta_n)$$
$$\sin\left(\frac{1}{2}\Gamma\right) - \frac{1}{2}\sin(\Gamma) > \sin\left[\frac{1}{2}(2\pi - \Gamma)\right] - \frac{1}{2}\sin(2\pi - \Gamma)$$
$$-\frac{1}{2}\sin(\Gamma) > \frac{1}{2}\sin(\Gamma).$$

Since $\sin(\Gamma) < 0, \forall\,\varepsilon \in (0, \frac{2\pi}{3})$, the above inequality holds and $\Delta A(\theta_{n_{\max}}) > \Delta A(\theta_n)$. ■

Theorem III.1 provides a simple recipe for the placement problem, which is summarized in Algorithm 1.

It is worth noting that several approaches have been developed in the literature specifying the optimal configuration of *all* available sensors to map a single target. In contrast, Theorem III.1 specifies the optimal placement of *one* additional receiver into an environment comprising *arbitrarily* placed, pre-deployed receivers. While these two problems are not directly comparable, in what follows, it is easy to verify that the op-

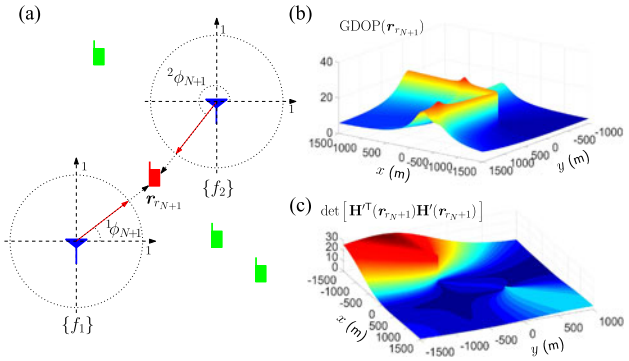

Fig. 4. (a) Environment comprised of 3 pre-deployed receivers (green) estimating the states of 2 unknown SOPs (blue). The optimal receiver placement problem is to place an additional receiver (red) at a position $\boldsymbol{r}_{r_{N+1}}$ that will minimize the GDOP (b) or maximize the determinant (c).

timal GDOP for the two-dimensional (2-D) environments found in [41] and [28] and the maximum logarithm of the FIM determinant in [37] is achieved by Algorithm 1 when the pre-deployed receivers reside at N of the vertices of an $(N+1)$-sided regular polygon. Specifically, there will be N angles sandwiched between consecutive receivers equal to $360/(N+1)$ and one angle equal to $2\times 360/(N+1)$. The largest angle $2\times 360/(N+1)$ is halved, which places the receiver anywhere on a ray passing through the remaining vertex of the regular polygon.

C. Case Two: Multiple SOPs

For planar environments comprising multiple SOPs, it is obvious that (6) and (7) can not be reparameterized over ${}^1\phi_{N+1}$ as was done in section III-B. As such, the optimization functions in (6) and (7) are over $\boldsymbol{r}_{N+1}$, and are neither convex nor concave. To see this, an environment comprising three pre-deployed receivers, a candidate receiver position, and two terrestrial SOPs is illustrated in Fig. 4(a). The resulting GDOP($\boldsymbol{r}_{r_{N+1}}$) and $\det[\mathbf{H}'^{\mathsf{T}}(\boldsymbol{r}_{r_{N+1}})\mathbf{H}'(\boldsymbol{r}_{r_{N+1}})]$ for placing an additional receiver at candidate positions on a grid sampled at one meter intervals in $[-1500,-1000]^{\mathsf{T}} \leq \boldsymbol{r}_{r_{N+1}} \leq [1500,1500]^{\mathsf{T}}$ are plotted in Fig. 4(b) and (c), respectively. The bounds on the grid $[-1500,-1000]^{\mathsf{T}}$ and $[1500,1500]^{\mathsf{T}}$ were chosen to center the environment for illustration purposes. In general, arbitrary bounds may be chosen. It is clear from these surfaces that (6) and (7) do not posses any useful convexity properties. In the following, the area maximization problem will be generalized and shown to yield a family of convex programs.

1) *Product of Areas Maximization:* Recall the block diagonal structure of the measurement Jacobian $\mathbf{H}' = \operatorname{diag}\left[\mathbf{H}'_1,\ldots,\mathbf{H}'_M\right]$ for environments comprising multiple SOPs. From this structure, it is readily seen that

$$\mathbf{H}'^{\mathsf{T}}\mathbf{H}' = \begin{bmatrix} \mathbf{H}_1'^{\mathsf{T}}\mathbf{H}'_1 & \mathbf{0}_{3\times 3} & \cdots & \mathbf{0}_{3\times 3} \\ \mathbf{0}_{3\times 3} & \mathbf{H}_2'^{\mathsf{T}}\mathbf{H}'_2 & \cdots & \mathbf{0}_{3\times 3} \\ \vdots & \vdots & \ddots & \vdots \\ \mathbf{0}_{3\times 3} & \mathbf{0}_{3\times 3} & \cdots & \mathbf{H}_M'^{\mathsf{T}}\mathbf{H}'_M \end{bmatrix}.$$

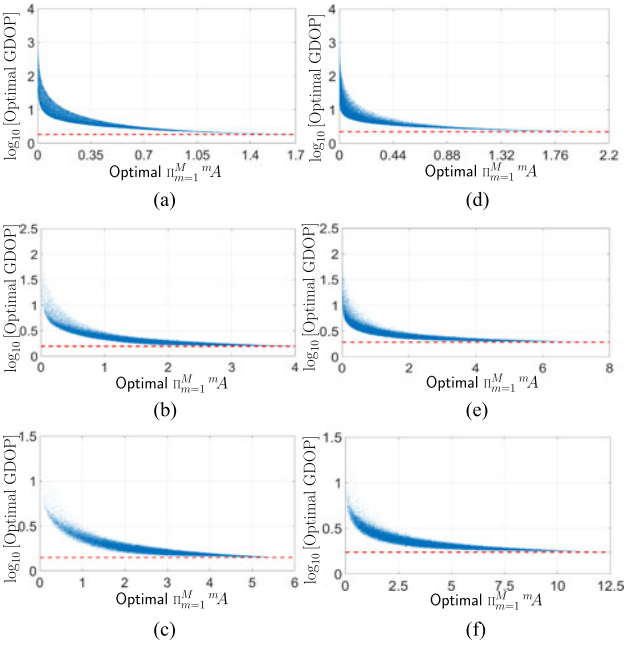

Fig. 5. N receivers were randomly placed around M SOPs for a total of 10^5 configurations. Next, the $(N+1)$st receiver was optimally placed so to first optimize the GDOP then to optimize the product of areas. Each point in the point cloud plotted in Fig. (a)–(f) represent the optimal product of areas versus optimal GDOP for a particular configuration. Fig. (a)–(c) correspond to $N=2,\ldots,4$, respectively, for $M=2$, and Fig. (d)–(f) corresponds to $N=2,\ldots,4$, respectively, for $M=3$. The minimum possible GDOP is plotted for each case (red dotted line).

By exploiting the block diagonal structure of $\mathbf{H}'^{\mathsf{T}}\mathbf{H}'$, the optimization problem in (7) can be rewritten as

$$\underset{\boldsymbol{r}_{r_{N+1}}}{\text{maximize}} \quad \prod_{m=1}^{M} \det\left[\mathbf{H}'^{\mathsf{T}}_m\left({}^m\phi_{r_{N+1}}\right)\mathbf{H}'_m\left({}^m\phi_{r_{N+1}}\right)\right]. \quad (14)$$

Note that the optimization problem in (7) for the single SOP case generalized to product of determinants in (14) for the multiple SOP case. As such, a natural extension of the area maximization problem in (8) to the multiple SOP case is to consider the product of each area ${}^mA$ of the polygon formed by the unit LOS vector endpoints pointing from the mth SOP to each receiver. To compare this optimization criterion with (6), $N+1$ receivers were placed randomly around multiple SOPs, where the nth receiver position was chosen according to $\boldsymbol{r}_{r_n} \sim \mathcal{U}([-1500,-1500]^{\mathsf{T}},[1500,1500]^{\mathsf{T}})$, for $n=1,\ldots,N$, for a total of 10^5 random configurations. For each configuration, the first N receivers were fixed. Next, the $(N+1)$st receiver was placed so to first optimize the GDOP then to optimize the product of areas. The corresponding GDOP and product of areas are plotted for $M=2$ in Fig. 5(a)–(c) for $N=2,\ldots,4$, respectively, and for $M=3$ in Fig. 5(d)–(f) for $N=2,\ldots,4$, respectively.

The following can be concluded from these plots. First, placing the $(N+1)$st receiver to optimize the product of areas approximately optimizes the GDOP and the loss in optimality is minimal, which is captured by the thickness of the "point cloud." The loss in optimality is

defined as the increase incurred in the GDOP from the optimal GDOP value due to optimizing the product of areas $\prod_{m=1}^{M} {}^{m}A$. Second, when $N+1$ receivers are arranged so the endpoints of the LOS vectors approach the formation of regular polygons for each SOP, the theoretical minimum GDOP, given by $\text{GDOP}_{\min} = \sqrt{5M/(N+1)}$ (dotted red line in Fig. 5), and maximum product of areas, given by $[(N+1)\sin[2\pi/(N+1)]/2]^{M}$ are simultaneously approached. Third, the potential loss in optimality is greater at smaller values of $\prod_{m=1}^{M} {}^{m}A$, which is attributed only to cases when all pre-deployed receivers are approximately collinear with an SOP.

Motivated by these results, an alternative optimization problem to (6) and (7) is proposed for $M > 1$, which aims to maximize the product of areas A_M over the position of the $(N+1)$st receiver, namely

$$\underset{\boldsymbol{r}_{r_{N+1}}}{\text{maximize}} \quad A_M\left(\boldsymbol{r}_{r_{N+1}}\right) = \prod_{m=1}^{M} {}^{m}A\left({}^{m}\phi_{N+1}\right). \tag{15}$$

Although (15) is not a convex optimization problem, it can be recast as a family of convex optimization problems by noting the following. First, by exploiting the preserving property of the logarithm, an equivalent optimization function is given by $\sum_{m=1}^{M} \log[{}^{m}A\,({}^{m}\phi_{N+1})]$. Second, recall from Fig. 2 that ${}^{m}A({}^{m}\phi_{N+1})$ is concave over ${}^{m}\phi_{N+1}$ in ${}^{m}\phi_{n} \le {}^{m}\phi_{N+1} \le {}^{m}\phi_{n+1}$, $n = 1, \ldots, N-1$. Third, the composition of a non-decreasing concave function, the logarithm, and a concave function, ${}^{m}A({}^{m}\phi_{N+1})$, is concave [41]. Fourth, the sum of concave functions is concave. Therefore, (15) can be recast as K convex optimization problems, each of which is the maximization of a concave function over a polyhedron S_k, specifically

$$\begin{aligned} \underset{\boldsymbol{r}_{r_{N+1}}}{\text{maximize}} \quad & \mathcal{J}_k\left(\boldsymbol{r}_{r_{N+1}}\right) = \sum_{m=1}^{M} \log\left[{}^{m}A\left({}^{m}\phi_{N+1}\right)\right] \\ \text{subject to} \quad & \mathrm{S}_k = \{\boldsymbol{r}_{r_{N+1}} \mid \mathbf{P}_k \boldsymbol{r}_{r_{N+1}} \preceq \boldsymbol{q}_k\}, \end{aligned} \tag{16}$$

for $\{\mathrm{S}_k\}_{k=1}^{K}$, where

$$\mathbf{P}_k = \begin{bmatrix} \boldsymbol{p}_{1,k}^{\mathsf{T}} \\ \vdots \\ \boldsymbol{p}_{L,k}^{\mathsf{T}} \end{bmatrix}, \quad \boldsymbol{q}_k = \begin{bmatrix} q_{1,k} \\ \vdots \\ q_{L,k} \end{bmatrix}.$$

It can be shown that K is upper-bounded by a classical equation related to the number of regions formed by intersecting lines, namely $K \le ([NM]^2 + [NM] + 2)/2$ [42]. The polyhedron S_k is formed by the intersection of L halfspaces, where $3 \le L \le NM$, and its geometry is determined by the positions of the receivers and SOPs [43]. The direction of the lth halfspace forming S_k is given by $-\boldsymbol{p}_{l,k}$, whereas $q_{l,k}$ accounts for the halfspace's offset from the origin of $\{f_1\}$. The inequality $\preceq$ denotes vector (componentwise) inequality. Fig. 6(a) is an illustration of these relationships for the same environment in Fig. 4(a). The resulting $\sum_{m=1}^{M} \log\,[{}^{m}A\,({}^{m}\phi_{N+1})]$ for this environment is plotted in Fig. 6(b). The family of K convex programs in (16) yields K receiver positions that are optimal over each

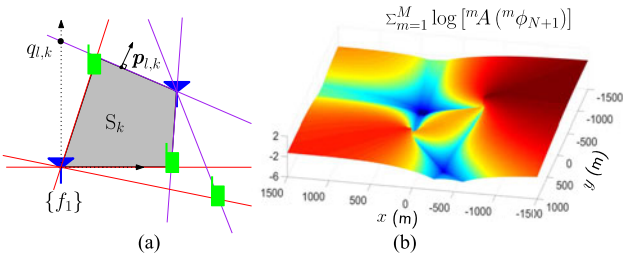

Fig. 6. (a) Environment comprising three pre-deployed receivers (green) estimating the states of two unknown SOPs (blue). The polyhedron set S_k (gray) is formed by the intersection of $L = 4$ halfspaces. The direction of the lth halfspace forming S_k is given by $-\mathbf{p}_{l,k}$. Each halfspace boundary is the line (purple and red) through each SOP to each receiver. For SOPs other than the reference frame SOP $\{f_1\}$, the resulting halfspace may not pass through the origin, which is captured by $q_{l,k}$.
(b) Resulting $\sum_{m=1}^{M} \log[{}^{m}A({}^{m}\phi_{N+1})]$ for placing an additional receiver at positions on a grid sampled at one meter intervals in $[-1500, -1000]^{\mathsf{T}} \le \boldsymbol{r}_{r_{N+1}} \le [1500, 1500]^{\mathsf{T}}$ into an environment comprised of three pre-deployed receivers and two SOPs.

S_k. Therefore, the global optimal solution $\mathcal{J}^{\star}$ is given by

$$\mathcal{J}^{\star}\left(\boldsymbol{r}^{\star}_{r_{N+1}}\right) = \max_{k}\left[\mathcal{J}_k^{\star}\left(\boldsymbol{r}^{\star}_{r_{N+1},k}\right)\right], \tag{17}$$

where the optimizer $\boldsymbol{r}^{\star}_{r_{N+1}}$ is the global optimal receiver position, and $\mathcal{J}_k^{\star}$ and $\boldsymbol{r}^{\star}_{r_{N+1},k}$ are the optimal value and the corresponding optimizer in the kth set, respectively. The above analysis provides a simple recipe for the optimal placement of an additional receiver into an environment comprising multiple, arbitrarily deployed SOPs, which is summarize in Algorithm 2.

2) *Convergence Analysis:* To solve the GDOP optimization problem, a nonlinear numerical optimization solver must be relied on. Due to the shape of the GDOP function in (6), the solver will often undesirably converge to a local optimal solution. To demonstrate this behavior, the environment in Fig. 4(a) was simulated and MATLAB's numerical nonlinear optimization function `fmincon` was used.

The solver's initial guess was drawn according to $\boldsymbol{r}_{r_{N+1}} \sim \mathcal{U}([-1500, -1000]^{\mathsf{T}}, [1500, 1500]^{\mathsf{T}})$ and the optimization problem was solved 10,000 times. In addition, the environment was gridded with a resolution $\Delta x = \Delta y = 1$ and the optimization problem was solved through exhaustive search to find the global minimum. The solution obtained through the numerical solver failed to converge to the global minimum 44.1% of the time.

The proposed optimization criterion (16), (17), while not directly optimizing GDOP, posses the following advantages. First, it decomposes the optimization problem into a family of independent convex programs, which may be executed in parallel. Second, the optimal solution of the optimization criterion (16), (17) is the global optimum to which the solver would converge in a faster fashion. Third, the obtained solution from (16), (17) is very "close" to the global solution of (6).

The global optimizer for the GDOP problem (6) turned out to be $\boldsymbol{r}^{\star}_{N+1} = [-1500, -630]^{\mathsf{T}}$, while the optimizer for

Algorithm 2: Optimal Receiver Placement for Multiple SOPs.

Given: Positions of N pre-deployed receivers and estimates of M SOPs' positions
for $m = 1, \ldots, M$

- **Place** the origin of a cartesian coordinate frame at the position of the mth SOP.
- **Calculate** the angles $\{{}^m\theta_n\}_{n=1}^N$ sandwiched between vectors pointing from the mth SOP to each receiver.
- **Parameterize** the area ${}^mA$ for the mth SOP by the candidate receiver position $\boldsymbol{r}_{N+1}$ using (27) in Appendix A.

end for
Divide the environment into K polyhedra using (28) and (29) in Appendix B.
for $k = 1, \ldots, K$

- **Initialize** receiver placement guess anywhere in set k.
- **Solve** the convex optimization problem (16) numerically.
- **Save** the optimal value $\mathcal{J}_k^\star$ and its optimizer $\boldsymbol{r}_{r_{N+1}^\star,k}$.

end for
Place the additional receiver at $\boldsymbol{r}^\star_{r_{N+1}}$ according to (17).

(16), (17) turned out to be $\boldsymbol{r}^\star_{N+1} = [-1500, -657]^{\mathsf{T}}$. The GDOP associated with the optimizer of (6) was 2.5517, while the GDOP evaluated at the optimizer of (16), (17) was 2.5518. It is worth noting that one could use the optimal solution from (16), (17) as a good initial guess that is close to the optimal solution of the GDOP problem (6).

IV. OPTIMAL MAPPING PERFORMANCE CHARACTERIZATION

This section characterizes the optimal mapping performance of an SOP as a function of the number of mobile receivers in the environment and time. The objective of this characterization is to prescribe the optimal achievable mapping performance of an SOP within a specified time and for a certain number of receivers.

A. Problem Formulation

The following problem is considered. A set of N mobile receivers with knowledge about their own states are making pseudorange observations on an unknown terrestrial SOP. Assuming that these observations are fused through a dynamic centralized estimator, specifically an extended Kalman filter (EKF), to estimate the state vector of the SOP $\boldsymbol{x}_s$ with dynamics (1), what is the optimal mapping performance as a function of N and time?

In contrast to Section III, which analyzed the optimal placement of the $(N+1)$st receiver, given a set of N randomly-distributed receivers, the optimal mapping performance for the problem considered here is a function of the simultaneous placement of all the receivers. Specifically, the optimization is over all the receiver angles $\{{}^1\phi_n\}_{n=1}^N$. This optimization enables an off-line characterization of the optimal achievable mapping performance, which is summarized in Theorem IV.1.

THEOREM IV.1 *The optimal mapping performance for N mobile receivers with knowledge of their own states collaboratively estimating the state vector of one terrestrial SOP with dynamics (2) using pseudorange observations (3) with independent noise with identical measurement noise variance σ^2 is: 1) independent of the SOP's state vector estimate and 2) solvable off-line. The optimal mapping performance is given by the solution to the discrete-time Riccati equation*

$$\begin{aligned}\mathbf{P}(k+1|k) = \mathbf{F}_s\big\{&\mathbf{P}(k|k-1) - \mathbf{P}(k|k-1)\mathbf{H}^{\star\mathsf{T}} \\ &\cdot \Big[\mathbf{H}^\star\mathbf{P}(k|k-1)\mathbf{H}^{\star\mathsf{T}} + \mathbf{R}\Big]^{-1} \\ &\cdot \mathbf{H}^\star\mathbf{P}(k|k-1)\big\}\mathbf{F}_s^{\mathsf{T}} + \mathbf{Q}_s \end{aligned} \tag{18}$$

with initial value $\mathbf{P}(0|-1)$, where $\mathbf{P}$ is the prediction error covariance,

$$\mathbf{H}^\star = \begin{bmatrix} -\cos\frac{2\pi 0}{N} & -\sin\frac{2\pi 0}{N} & -1 & 0 \\ -\cos\frac{2\pi}{N} & -\sin\frac{2\pi}{N} & -1 & 0 \\ \vdots & \vdots & \vdots & \vdots \\ -\cos\frac{2\pi(N-1)}{N} & -\sin\frac{2\pi(N-1)}{N} & -1 & 0 \end{bmatrix}, \tag{19}$$

the matrix $\mathbf{R}$ is the measurement noise covariance, and $\mathbf{F}_s$ and $\mathbf{Q}_s$ are the SOP's state dynamics and process noise covariance, respectively, which are defined in section II-A.

PROOF Assuming the receivers' observation noise to be i.i.d., i.e., $\{\sigma_n^2\}_{n=1}^N \equiv \sigma^2$ and $\mathbf{R} = \sigma^2\mathbf{I}_{N\times N}$, the optimal achieved performance is essentially determined by the geometric placement of the receivers. The lowest GDOP is achieved when the unit LOS vectors pointing from the SOP to the receivers reside at the vertices of a regular polygon [28]. Therefore, an environment consisting of N optimally-placed receivers, each drawing pseudorange observations on the same SOP modifies the observation Jacobian matrix for (3) to take the form of (19).

Next, consider the estimation error covariance update equation of the EKF in the information form

$$\mathbf{P}^{-1}(k+1|k+1) = \mathbf{P}^{-1}(k+1|k) + \frac{1}{\sigma^2}\mathbf{H}^{\mathsf{T}}(k+1)\mathbf{H}(k+1),$$

where $\mathbf{P}(k+1|k+1)$ is the estimation error covariance and $\mathbf{P}(k+1|k)$ is the prediction error covariance. The information associated with the latest observation (at time step $k+1$) is $\boldsymbol{\Upsilon}(k+1) \triangleq \frac{1}{\sigma^2}\mathbf{H}^{\mathsf{T}}(k+1)\mathbf{H}(k+1)$. If the receivers are placed optimally, plugging (19) into $\boldsymbol{\Upsilon}(k+1)$

yields

$$\boldsymbol{\Upsilon}(k+1) = \frac{1}{\sigma^2}\sum_{n=0}^{N-1}\begin{bmatrix} \cos^2\frac{2\pi n}{N} & \cos\frac{2\pi n}{N}\sin\frac{2\pi n}{N} & \cos\frac{2\pi n}{N} & 0 \\ \sin\frac{2\pi n}{N}\cos\frac{2\pi n}{N} & \sin^2\frac{2\pi n}{N} & \sin\frac{2\pi n}{N} & 0 \\ \cos\frac{2\pi n}{N} & \sin\frac{2\pi n}{N} & 1 & 0 \\ 0 & 0 & 0 & 0 \end{bmatrix}. \tag{20}$$

By using the Fourier equations

$$\sum_{n=0}^{N-1}\cos^2\frac{2\pi n}{N} = \frac{N}{2}, \quad \sum_{n=0}^{N-1}\sin^2\frac{2\pi n}{N} = \frac{N}{2},$$
$$\sum_{n=0}^{N-1}\cos\frac{2\pi n}{N}\sin\frac{2\pi n}{N} = 0,$$

and the summation equations

$$\sum_{n=0}^{N-1}\cos\frac{2\pi n}{N} = 0, \quad \sum_{n=0}^{N-1}\sin\frac{2\pi n}{N} = 0,$$

the information (20) becomes

$$\boldsymbol{\Upsilon}(k+1) = \frac{1}{\sigma^2}\text{diag}\left[\frac{N}{2}, \frac{N}{2}, N, 0\right],$$

which is independent of the SOP's state vector estimate. Noting that the SOP's dynamics are linear, the prediction error covariance, given by

$$\mathbf{P}(k+1|k) = \mathbf{F}_s\mathbf{P}(k|k)\mathbf{F}_s^{\mathrm{T}} + \mathbf{Q}_s,$$

is also independent of the SOP's state vector estimate. Therefore, if the receivers maintain their optimal distribution around the latest SOP's position estimate $\hat{\boldsymbol{r}}_s$ at the time instants when new observations are taken, the estimation error covariance can be computed without knowledge of the SOP's state vector estimates. This allows for solving the Riccati equation (18) governing the evolution of the estimation error covariance off-line, and the resulting estimation error covariance time history is the optimal mapping performance as a function of time and number of receivers N. ■

B. Simulation Results

This section presents simulation results demonstrating the optimal mapping performance as a function of time and N. Moreover, the estimation error due to random receiver trajectories is compared with the optimal mapping performance. The simulation settings are summarized in Table I.

Fig. 7 illustrates the logarithm of the determinant of the posterior estimation error covariance, $\log\{\det[\mathbf{P}^{\star}(k+1|k+1)]\}$, which is related to the volume of the estimation uncertainty ellipsoid [24], as a function of time and N. This plot provides the minimum achievable uncertainty of the states of an unknown SOP as a function of time and N. This plot can be utilized to determine the minimum number of receivers that must be deployed in an environment to achieve a desired estimation uncertainty within a specified period of time.

TABLE I
Simulation Settings for Optimal Mapping Performance of an Unknown SOP

Parameter	Value
$\boldsymbol{x}_s(0)$	$[0, 0, 1, 0.1]^{\mathrm{T}}$
$\mathbf{P}_s(0\|-1)$	$(10^3)\cdot\text{diag}\,[1, 1, 3, 0.3]$
$\hat{\boldsymbol{x}}_s(0\|-1)$	$\sim\mathcal{N}[\boldsymbol{x}_s(0), \mathbf{P}_s(0\|-1)]$
$\{h_{0,s}, h_{-2,s}\}$	$\{8.0\times10^{-20}, 4.0\times10^{-23}\}$
σ^2	$100\,\text{m}^2$
T	0.1 s

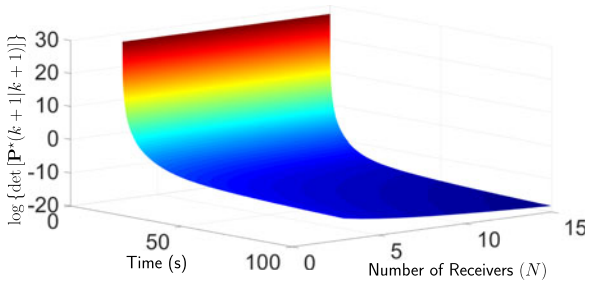

Fig. 7. Logarithm of the determinant of the optimal posterior estimation error covariance $\log\{\det[\mathbf{P}^{\star}(k+1|k+1)]\}$ expressed as a function of time and $N \in \{3, 4, \ldots 15\}$ receivers.

TABLE II
Simulation Settings for the Receivers' Initial Position

Parameter	Value
$\boldsymbol{r}_{r_1}^j(0)$	$[-150.8, 169.3]^{\mathrm{T}} + \boldsymbol{b}_j$
$\boldsymbol{r}_{r_2}^j(0)$	$[24.6, -13.7]^{\mathrm{T}} + \boldsymbol{b}_j$
$\boldsymbol{r}_{r_3}^j(0)$	$[-25.6, -45.5]^{\mathrm{T}} + \boldsymbol{b}_j$
$\boldsymbol{r}_{r_4}^j(0)$	$[105.7, -29.6]^{\mathrm{T}} + \boldsymbol{b}_j$
$\boldsymbol{b}_1, \boldsymbol{b}_2, \boldsymbol{b}_3$	$[0, 0]^{\mathrm{T}}, [125, 0]^{\mathrm{T}}, [200, 0]^{\mathrm{T}}$

To compare the optimal mapping performance versus random receiver trajectories that do not maintain the optimal receiver placement around the SOP's position estimate, four receivers were randomly placed around the SOP. The initial state vector of the nth receiver was set to $\boldsymbol{x}_{r_n}(0) = [\boldsymbol{r}_{r_n}^{\mathrm{T}}(0), \dot{\boldsymbol{r}}_{r_n}^{\mathrm{T}}(0), c\delta t_{r_n}(0), c\dot{\delta} t_{r_n}(0)]^{\mathrm{T}}$, where $\dot{\boldsymbol{r}}_{r_n}(0) = [0, 0]^{\mathrm{T}}$, $c\delta t_{r_n}(0) = 10$, and $c\dot{\delta} t_{r_n}(0) = 1$. The receivers' initial positions $\boldsymbol{r}_{r_n}(0)$ are specified in Table II. The receivers' initial positions were varied across three simulation runs, by varying an offset $\{\boldsymbol{b}_j\}_{j=1}^3$ to create varying GDOP quality. Subsequently, the receivers moved according to a velocity random walk motion with an acceleration process noise power spectral density $\tilde{q}_x = \tilde{q}_y = 0.1(\text{m/s}^2)^2$ [13]. The receivers' trajectories across the three simulation runs (corresponding to $j = 1, 2, 3$) were the same in order to analyze the effect of the initial GDOP. The time history of the resulting $\log\{\det[\mathbf{P}^j(k+1|k+1)]\}$ corresponding to $j = 1, 2, 3$ versus the optimal $\log\{\det[\mathbf{P}^{\star}(k+1|k+1)]\}$ are plotted in Fig. 8(a) for the trajectories traversed plotted in Fig. 8(b)–(d).

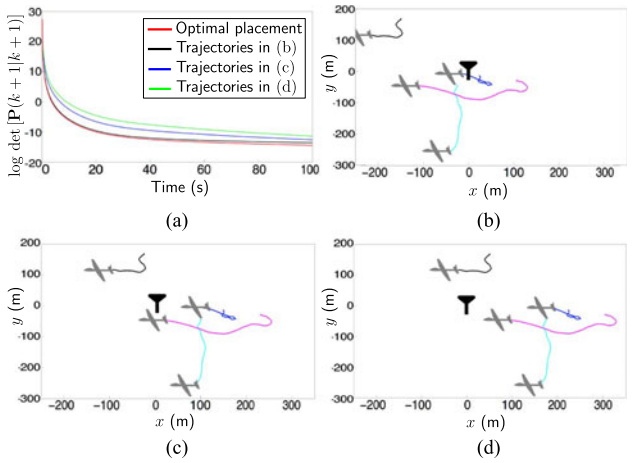

Fig. 8. Logarithm of the determinant of the optimal posterior estimation error covariance $\log\left\{\det\left[\mathbf{P}^{\star}(k+1|k+1)\right]\right\}$ versus the posterior estimation error covariance due to three simulation runs corresponding to the receiver trajectories in (b)–(d). The receivers' trajectories in (b)–(d) are the same. The receivers' initial positions in (b)–(d) were varied according to an offset $\boldsymbol{b}_j$ to yield different initial GDOP quality: (b) low GDOP with $\boldsymbol{b}_1$, (c) medium GDOP with $\boldsymbol{b}_2$, and (d) high GDOP with $\boldsymbol{b}_3$.

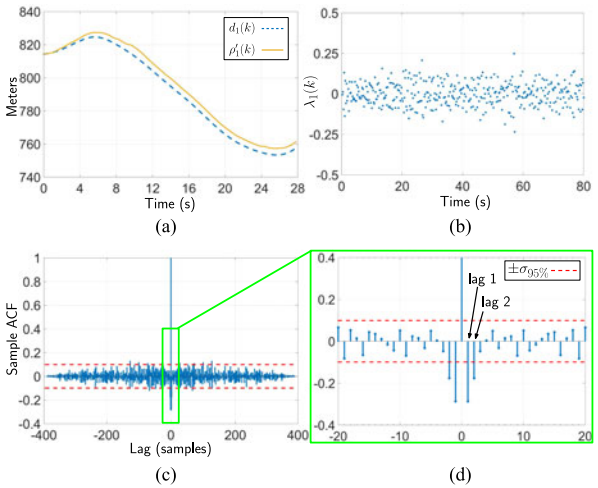

Fig. 9. Measurement analysis. (a) Comparison of the true data produced by the MATRIX SDR, ρ_1', and the distance from the receiver to the BTS, d_1. (b) The sequence (22) computed by replacing z_n' with the true data ρ_1'. (c) Resulting sample ACF of the sequence in (b) with the corresponding $\pm\sigma_{95\%}$ confidence bounds. (d) Zoom of (c) illustrating that only values up to the first two lags of the sample ACF are significant.

It can be seen from Fig. 8 that although the shape of the trajectories were the same between each run, the initial GDOP quality greatly influenced the resulting estimation uncertainty. Also note that although the trajectories in Fig. 8(b) corresponded to the lowest initial GDOP out of all the runs, the resulting estimation uncertainty for these trajectories never violated the optimal $\log\{\det[\mathbf{P}^{\star}(k+1|k+1)]\}$.

V. EXPERIMENTAL RESULTS

This section demonstrates collaborative mapping of a terrestrial SOP emanating from a cellular CDMA base transceiver station (BTS). This section consists of two sections. In the first section, the dynamics and observation models presented in Section II are validated to be suitable models in a real-world setting. Such model validation is crucial, since these models were used in deriving the optimal collaborative mapping performance of the EKF in Theorem IV.1. In the second section, collaborative mapping results demonstrate the bound derived in Theorem IV.1. To this end, three vehicles were equipped with two antennas each, to acquire and track multiple GPS signals and a cellular BTS whose signal was modulated through CDMA. The GPS and cellular signals were simultaneously downmixed and synchronously sampled via two National Instruments® universal software radio peripherals (USRPs). These front-ends fed their data to the generalized radionavigation interfusion device software-defined radio (SDR) [44] and the Multichannel Adaptive TRansceiver Information eXtractor (MATRIX) SDR [15], which produced pseudorange observables from all GPS L1 C/A signals in view and the cellular BTS, respectively, at $1/T = 5$Hz. Fig. 10 depicts the experimental hardware setup.

The MATRIX SDR produced pseudorange observables to the BTS, modeled according to (3), by exploiting the cellular CDMA signal structure as described in detail in [15]. The produced pseudoranges are unambiguous in the sense that they were associated with a particular BTS by decoding the BTS's identification number from the cellular CDMA paging channel. For this field experiment, the SOP's signal structure was known to be cellular CDMA. If the signal structure is unknown, several SDR modules (e.g., CDMA, LTE, FM, etc.) may be run in parallel until a LOS signal is acquired and tracked and data association for the produced pseudorange and the SOP transmitter is performed. If the receiver is in an environment subject to multipath, one of several multipath mitigation methods can first be employed to improve the LOS time-of-arrival estimate, e.g., estimation of signal parameters via rotational invariance (ESPRIT) [45] and space-alternating generalized expectation maximization (SAGE) [46].

A. Model Verification

The symbol ρ_n will be used to denote the nth receiver's produced pseudorange measurement (i.e., data by the MATRIX SDR) to contrast the pseudorange model z_n in (3). Consider the nth receiver's clock bias-compensated pseudorange observation model

$$z_n'(k) \triangleq z_n(k) - c\delta t_r(k) = d_n(k) - c\delta t_s(k) + v_n(k), \quad (21)$$

where $d_n(k) \triangleq \|\boldsymbol{r}_{r_n}(k) - \boldsymbol{r}_s\|$. According to (21), the MATRIX SDR's clock bias-compensated pseudorange $\rho_n'(k) \triangleq \rho_n(k) - c\delta t_{r_n}(k)$ should consist of d_n, $c\delta t_s$, and v_n. To analyze this, a vehicle traversed a trajectory for 28 s while producing ρ_1 to a single BTS. The receiver's states $c\delta t_{r_1}$ and $\boldsymbol{r}_{r_1}$ were estimated by a least-squares solver using the available GPS pseudoranges and the position $\boldsymbol{r}_s$ was surveyed from the BTS's true location. The true data ρ_1' and the distance d_1 are plotted in Fig. 9(a). The initial value $\rho_1'(0)$ was aligned with $d_1(0)$ to compensate for $c\delta t_s(0)$.

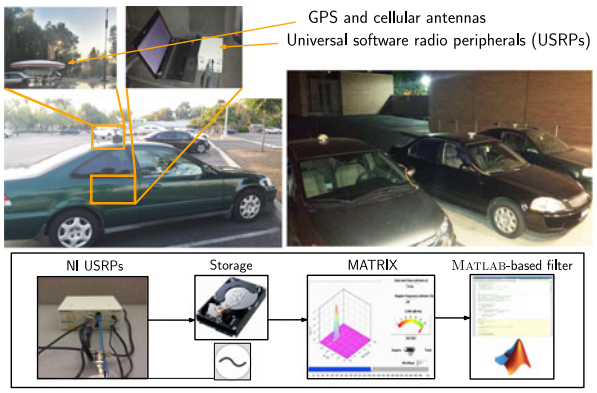

Fig. 10. Experiment hardware setup.

From Fig. 9(a) it can be noted that the profiles of the curves closely match, indicating that the trend of ρ_1 is mainly due to d_1. The receiver's clock bias-compensated observation model (21) suggests that the deviation of ρ_1' from d_1 is attributed to v_n and the dynamics of $c\delta t_s$. To verify this deviation, the measurement noise v_n and the process noise terms $w_{\delta t_s}$ and $w_{\dot{\delta} t_s}$ driving $c\delta t_s$ and $c\dot{\delta} t_s$ are studied next by applying the following steps commonly used in time-series analysis [47]. First, the data is de-trended by subtracting d_n and applying a transformation to obtain stationary residuals, specifically, a linear combination of $w_{\delta t_s}$, $w_{\dot{\delta} t_s}$, and v_n. Second, the sample autocorrelation function (ACF) is computed for the resulting sequence. Third, an appropriate model is identified by using key attributes from the sample ACF and is compared with the model presented in this paper.

The transformation applied is a double-difference in time defined by $\lambda_n(k+1) \triangleq \gamma_n(k+1) - \gamma_n(k)$, where $\gamma_n(k+1) \triangleq \bar{z}(k+1) - \bar{z}(k)$ and $\bar{z}(k) \triangleq d_n(k) - z_n'(k)$. It is shown in Appendix C that $\lambda_n(k)$ has the form

$$\lambda_n(k) = \lambda_{n,1}(k) + \lambda_{n,2}(k) + \lambda_{n,3}(k), \tag{22}$$

where $\lambda_{n,1}(k) \triangleq w_{\delta t_s}(k) - w_{\delta t_s}(k-1)$, $\lambda_{n,2}(k) \triangleq -[v_n(k) - 2v_n(k-1) + v_n(k-2)]$, and $\lambda_{n,3}(k) \triangleq T w_{\dot{\delta} t_s}(k)$. The sequences $\lambda_{n,1}$ and $\lambda_{n,2}$ are first-order and second-order moving averages (MAs), respectively, which have the form

$$\xi_i(k) = \sum_{j=0}^{q_i} \beta_j e(k-j), \quad \beta_0 = 1,$$

where β_j is a constant, e is a DT zero-mean white noise sequence, and q_i is the MA order [48]. The sequence $\lambda_{n,3}$ is a DT zero-mean white noise sequence, which can be generalized as an MA with order $q_3 = 0$. It follows that λ_n itself is an MA, since the sum of MAs is also an MA with order $q \leq \max\{q_1, q_2, q_3\} = 2$, where q_i is the order of $\lambda_{n,i}$ [49].

The sample ACF of a qth order MA will have significant values up to lag q, and will become effectively zero thereafter. Effectively zero implies that the sample ACF values should be approximately zero-mean and obey the 95th-percentile confidence bounds ($\pm\sigma_{95\%} \approx \pm 1.96/\sqrt{L}$), where L is the total number of samples [48]. To check if the collected data agrees with this hypothesis, z_n' was replaced with ρ_1' to produce λ_1, which is plotted in Fig. 9(b). The sample ACF of λ_1 and the corresponding $\pm\sigma_{95\%}$ bounds are plotted in Fig. 9(c) and (d) for $L = 400$ samples.

The following conclusions about the underlying sequences can be noted from Fig. 9(c) and (d). First, since the last significant ACF value is at the second lag, a second order MA model is appropriate, as hypothesized. Second, since an MA model is appropriate, the driving process noise $w_{\delta t_s}$ and $w_{\dot{\delta} t_s}$ and the measurement noise v_n are appropriately modeled as white sequences. Third, since a double-difference in time was required to detrend the data, a double-integrator SOP clock model is appropriate. Fourth, since λ_n is a stationary MA and by invoking a second-order ergodicity assumption, the measurement noise variance σ_n^2 can be computed from the data, as is shown in Appendix D, to be

$$\sigma_n^2 = \frac{1}{6}\mathrm{var}_L(\lambda_n) - \frac{1}{3}c^2\left(S_{\tilde{w}_{\delta t_s}} T + S_{\tilde{w}_{\dot{\delta} t_s}} \frac{T^3}{3}\right), \tag{23}$$

where $\mathrm{var}_L(\lambda_n)$ is the sample variance of λ_n using L samples.

B. Mapping Results

Three separate runs were conducted. In the first run, the vehicle-mounted receivers began their trajectories in positions that resulted in a low GDOP. The receivers began estimating the states of the cellular BTS $\boldsymbol{x}_s$ by fusing their pseudorange observables through a centralized EKF. The network implementation to fuse these pseudoranges could be integrated into developing communication standards, such as the IEEE802.11p dedicated short range communication, which is designed to support future vehicle-to-vehicle and vehicle-to-infrastructure communication [50].

The EKF was initialized with an initial estimate given by $\hat{\boldsymbol{x}}_s(0|-1) \sim \mathcal{N}[\boldsymbol{x}_s(0), \mathbf{P}_s(0|-1)]$, where $\boldsymbol{x}_s(0) = [\boldsymbol{r}_s^{\mathrm{T}}(0), c\delta t_s(0), c\dot{\delta} t_s(0)]^{\mathrm{T}}$, where $\boldsymbol{r}_s(0)$ is the projection of the BTS's true position in the earth-centered earth-fixed coordinate frame to a planar system, $c\delta t_s(0) \equiv d_1(0) + c\delta t_{r_1}(0) - \rho_1(0)$, $c\dot{\delta} t_s(0) \equiv [c\delta t_s(1) - c\delta t_s(0)]/T$, and $\mathbf{P}_s(0|-1) \equiv (10^4) \cdot \mathrm{diag}[1, 1, 3, 0.3]$. This initialization scheme is customary in EKFs in which the prior, uncertain information is utilized. Other initialization schemes are also possible. For example, a batch nonlinear least-squares-type approach could be employed in which a batch of initial measurements are used to produce an initial guess $\hat{\boldsymbol{x}}_s(0|-1)$ and associated $\mathbf{P}_s(0|-1)$. Alternatively, a particle filter operating on a batch of measurements could be employed to produce $\hat{\boldsymbol{x}}_s(0|-1)$ and $\mathbf{P}_s(0|-1)$. The particles could be initialized by drawing positions from a polar coordinate system fixed at each receiver with an angle drawn uniformly between 0 and 2π and a radius drawn uniformly between 0 and the maximum operating range of the cellular BTS. The initial clock bias for each particle may be computing using the initial measurements and the drawn position, while the clock drift for each particle could be initialized to zero. It is worth noting that since three

Fig. 11. Experimental results for low GDOP run. Image: Google Earth.

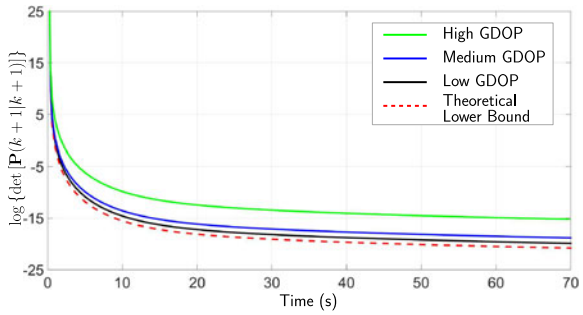

Fig. 12. Resulting log {det [$\mathbf{P}(k+1|k+1)$]} produced by the EKF for each of the three experimental runs plotted against the theoretical lower bound (red dotted curve), which was found using Theorem IV.1. The black curve corresponds to low GDOP calculated from the receiver positions illustrated in Fig. 11. The blue and green curves correspond to medium and high GDOP, respectively, which were calculated from the second and third experimental runs, respectively.

noncollinear receivers were collaboratively mapping the 2-D position of a BTS, there will be no local observability issues with the EKF and the estimates will be unambiguous.

The process noise covariance for the BTS's oscillator $\mathbf{Q}_{\text{clk},s}$ was assumed to correspond to a typical oven-controlled crystal oscillator, which is usually the case for cellular CDMA BTSs [12]. Any mismatch between the true $\mathbf{Q}_{\text{clk},s}$ and the assumed one will be small and will be included in the measurement noise variances $\{\sigma_n^2\}_{n=1}^3$. Alternatively, $\mathbf{Q}_{\text{clk},s}$ could be estimated off-line through a batch estimator or online adaptively [51]. The measurement noise variances $\{\sigma_n^2\}_{n=1}^3$ were calculated using (23) as described in section V-A. These values were found to be very similar, i.e., $\{\sigma_n^2\}_{n=1}^3 \approx \sigma^2$. Moreover, the receivers were placed sufficiently far from each other to assume independent channels between the BTS and each receiver. Therefore, the measurement noise covariance was set to $\mathbf{R} \equiv \sigma^2 \mathbf{I}_{3\times 3}$.

The final 2-D estimation error of the BTS's position was within 3 m from the true BTS position after 70 s. Fig. 11 is an illustration of the receivers' trajectories, the true and estimated BTS position, and the initial and final 95th-percentile estimation uncertainty ellipses of $\hat{\boldsymbol{r}}_s$ for the low GDOP run. Note from Fig. 11 the significant reduction in the size of estimation uncertainty ellipse from the initial to the final uncertainty with only three receivers. The black curve in Fig. 12 illustrates the corresponding time history of log{det[$\mathbf{P}(k+1|k+1)$]} plotted against the theoretical lower bound that was found in Section IV. In the second and third runs, the receivers were initialized in positions that resulted in a medium and high GDOP, respectively. A summary of the mapping errors for each run are tabulated in Table III. The 3 m localization is dependent on many factors (e.g., type of transmitter being mapped, noise statistics, number of receivers and corresponding trajectories, elapsed time, etc.). The resulting time history of log{det[$\mathbf{P}(k+1|k+1)$]} are plotted as the blue and green curves in Fig. 12. Comparable results were noted upon running the EKF with different initial estimates. These experimental results demonstrate the expected behavior of: 1) a worse quality mapping performance for receiver positions yielding higher GDOP and 2) none of the traversed trajectories resulted in an estimation uncertainty which violated the theoretical optimal mapping performance (lower-bound).

TABLE III
Final BTS Position Errors

Initial GDOP	Low (3.8)	Medium (8.5)	High (12.4)
Mapping Error (m)	3.0	4.7	6.9

VI. CONCLUSION

This paper studied optimal collaborative mapping of terrestrial SOPs. First, the optimal placement of a receiver to an environment comprising one SOP and N pre-deployed receivers with a random initial distribution was considered. Three optimization problems were formulated and compared: minimizing the GDOP, maximizing the determinant of the inverse of the GDOP matrix, and maximizing the area of a polygon inscribed in the unit circle whose vertices are the endpoints of unit LOS vectors from the SOP to the receivers. It was shown that the area maximization problem is piecewise-concave with a simple analytical solution. Next, the optimal receiver placement problem was extended to an environment comprising an arbitrary number of SOPs. A novel optimization criterion was proposed for this scenario, namely, the sum of logarithms of polygon areas. It was demonstrated that while the classical GDOP and determinant optimization problems do not posses any useful convexity properties, the proposed optimization criterion 1) yields a family of convex programs and guarantees a global optimal solution and 2) allows for executing the solver of the family of convex programs in parallel. This paper also derived the optimal mapping performance of a single SOP as a function of time and number of receivers in the environment and demonstrated the theoretical optimal mapping performance numerically and experimentally.

APPENDIX A
DERIVATION OF THE AREA OPTIMIZATION FUNCTION (16)

The resulting area ${}^mA\left({}^m\phi_{N+1}\right)$ for the mth SOP after placing the $(N+1)$st is

$$ {}^mA\left({}^m\phi_{N+1}\right) = {}^mA_N + \Delta^mA\left({}^m\phi_{N+1}\right), \qquad (24) $$

where ${}^mA_N$ is the area created by the pre-deployed receivers and $\Delta^mA\,({}^m\phi_{N+1})$ is the change in area from introducing the $(N+1)$st receiver, and is given by

$$\Delta^mA\left({}^m\phi_{N+1}\right) = \frac{1}{2}\big[\sin({}^m\phi_{N+1} - {}^m\phi_n) + \sin({}^m\theta_n - {}^m\phi_{N+1} + {}^m\phi_n) - \sin({}^m\theta_n)\big]. \tag{25}$$

Using the angle difference identity for the sine function, $\sin(\alpha-\beta) = \sin\alpha\cos\beta - \cos\alpha\sin\beta$, (25) can be rewritten as

$$\begin{aligned}\Delta^mA&\left({}^m\phi_{N+1}\right)\\ &= \frac{1}{2}\Big\{\big[\sin({}^m\phi_{N+1})\cos({}^m\phi_n) - \cos({}^m\phi_{N+1})\sin({}^m\phi_n)\big]\\ &\quad + \big[\sin({}^m\theta_n + {}^m\phi_n)\cos({}^m\phi_{N+1})\\ &\quad - \cos({}^m\theta_n + {}^m\phi_n)\sin({}^m\phi_{N+1})\big] - \sin({}^m\theta_n)\Big\}.\end{aligned} \tag{26}$$

The optimization function (24) can be parameterized by the candidate additional receiver position $\boldsymbol{r}_{N+1}$ by substituting the equality $[\cos({}^m\phi_n), \sin({}^m\phi_n)]^{\mathsf{T}} = \frac{\boldsymbol{r}_{r_n} - \hat{\boldsymbol{r}}_{s_m}}{\|\boldsymbol{r}_{r_n} - \hat{\boldsymbol{r}}_{s_m}\|}$ into (26) and substituting the result into (24), giving

$$\begin{aligned}{}^mA&\left(\boldsymbol{r}_{N+1}\right)\\ &= \frac{1}{2}\left\{\frac{(x_{r_{N+1}} - \hat{x}_{s_m})}{\|\boldsymbol{r}_{r_n} - \hat{\boldsymbol{r}}_{s_m}\|}\big[\sin({}^m\theta_n + {}^m\phi_n) - \sin({}^m\phi_n)\big]\right.\\ &\quad + \frac{(y_{r_{N+1}} - \hat{y}_{s_m})}{\|\boldsymbol{r}_{r_n} - \hat{\boldsymbol{r}}_{s_m}\|}\big[\cos({}^m\phi_n) - \cos({}^m\theta_n + {}^m\phi_n)\big]\\ &\quad \left. - \sin({}^m\theta_n)\right\} + {}^mA_N.\end{aligned} \tag{27}$$

Note that since ${}^mA_N$ is independent of $\boldsymbol{r}_{N+1}$, it may be omitted from the optimization problem. Its values can be computed off-line if desired.

APPENDIX B
EQUATIONS OF THE POLYHEDRA CONSTRAINTS (16)

The direction of the lth halfspace forming the polyhedron S_k is defined by the outward normal vector $-\boldsymbol{p}_{l,k}$, which is determined by the position of the nth pre-deployed receiver and the position estimate of the mth SOP, specifically

$$\boldsymbol{p}_{l,k} = \pm\left[-\frac{(y_{r_{N+1}} - \hat{y}_{s_m})}{\|\boldsymbol{r}_{r_n} - \hat{\boldsymbol{r}}_{s_m}\|}, \frac{\left(x_{r_{N+1}} - \hat{x}_{s_m}\right)}{\|\boldsymbol{r}_{r_n} - \hat{\boldsymbol{r}}_{s_m}\|}\right]^{\mathsf{T}}. \tag{28}$$

The corresponding halfspace's offset from the origin of $\{f_1\}$ is

$$q_{l,k} = y_{r_n} - \frac{(\hat{y}_{s_m} - y_{r_n})}{(\hat{x}_{s_m} - x_{r_n})}\cdot x_{r_n}. \tag{29}$$

APPENDIX C
DERIVATION OF (22)

Given the pseudorange observations z_n defined in (3), define

$$\begin{aligned}\bar{z}_n(k) &\triangleq \|\boldsymbol{r}_{r_n}(k) - \boldsymbol{r}_s\| + c\delta t_{r_n}(k) - z_n(k)\\ &= c\delta t_s(k) - v_n(k).\end{aligned} \tag{30}$$

The clock bias δt_s can be removed by a single difference of (30) in time and substituting for the SOP's DT clock bias dynamics $c\delta t_s(k+1) = c\delta t_s(k) + cT\dot{\delta t}_s(k) + w_{\delta t_s}(k)$, yielding

$$\begin{aligned}\gamma_n(k+1) &\triangleq \bar{z}_n(k+1) - \bar{z}_n(k)\\ &= c\delta t_s(k+1) - c\delta t_s(k) - [v_n(k+1) - v_n(k)]\\ &= cT\dot{\delta t}_s(k) + w_{\delta t_s}(k) - [v_n(k+1) - v_n(k)].\end{aligned} \tag{31}$$

The clock drift $\dot{\delta t}_s$ can be removed by a single difference of (31) in time and substituting for the SOP's clock drift dynamics $c\dot{\delta t}_s(k) = c\dot{\delta t}_s(k-1) + w_{\dot{\delta t}_s}(k-1)$, which yields

$$\begin{aligned}\lambda_n(k+1) &\triangleq \gamma_n(k+1) - \gamma_n(k)\\ &= cT[\dot{\delta t}_s(k) - \dot{\delta t}_s(k-1)] + [w_{\delta t_s}(k) - w_{\delta t_s}(k-1)]\\ &\quad - [v_n(k+1) - 2v_n(k) + v_n(k-1)]\\ &= Tw_{\dot{\delta t}_s}(k-1) + w_{\delta t_s}(k) - w_{\delta t_s}(k-1)\\ &\quad - [v_n(k+1) - 2v_n(k) + v_n(k-1)].\end{aligned}$$

Note that λ_n is the sum of three stationary sequences. For the sample ACF analysis conducted in this paper, each stationary sequence can be shifted to start with index k, giving

$$\lambda_n(k) = \lambda_{n,1}(k) + \lambda_{n,2}(k) + \lambda_{n,3}(k) \tag{32}$$

where $\lambda_{n,1}(k) \triangleq w_{\delta t_s}(k) - w_{\delta t_s}(k-1)$, $\lambda_{n,2}(k) \triangleq -[v_n(k) - 2v_n(k-1) + v_n(k-2)]$, and $\lambda_{n,3}(k) \triangleq Tw_{\dot{\delta t}_s}(k)$.

APPENDIX D
DERIVATION OF (23)

Equation (32) can be written as $\lambda_n(k) = \boldsymbol{\kappa}^{\mathsf{T}}\boldsymbol{y}(k)$ where

$$\boldsymbol{\kappa} \triangleq [1, T, -1, -1, 2, -1]^{\mathsf{T}},$$

$$\boldsymbol{y}(k) \triangleq \left[w_{\delta t_s}(k),\ w_{\dot{\delta t}_s}(k),\ w_{\delta t_s}(k-1),\ v_n(k),\ v_n(k-1),\ v_n(k-2)\right]^{\mathsf{T}}.$$

Assuming second-order ergodicity, i.e., for a sufficiently large number of samples L, the sample variance of λ_n, denoted $\mathrm{var}_L(\lambda_n)$, is equal to the ensemble variance and is given by

$$\mathrm{var}_L(\lambda_n) = \boldsymbol{\kappa}^{\mathsf{T}}\boldsymbol{\Sigma}\boldsymbol{\kappa}, \tag{33}$$

where $\boldsymbol{\Sigma} \triangleq \mathrm{cov}(\boldsymbol{y}) = \mathrm{diag}\left[c^2\mathbf{Q}_{\mathrm{clk},s}, c^2b, \sigma_n^2\mathbf{I}_{3\times3}\right]$ and $b \triangleq S_{\tilde{w}_{\delta t_s}}T + S_{\tilde{w}_{\dot{\delta t}_s}}\frac{T^3}{3}$ is the top left element of $\mathbf{Q}_{\mathrm{clk},s}$. Finally, using (33) to solve for $\sigma_{r_n}^2$ gives

$$\begin{aligned}6\sigma_{r_n}^2 &= \mathrm{var}_L(\lambda_n) - c^2\left(2TS_{\tilde{w}_{\delta t_s}} + \frac{2}{3}T^3S_{\tilde{w}_{\dot{\delta t}_s}}\right)\\ \Rightarrow \sigma_{r_n}^2 &= \frac{1}{6}\mathrm{var}_L(\lambda_n) - \frac{1}{3}c^2b.\end{aligned}$$

ACKNOWLEDGEMENT

The authors would like to thank J. Khalife, S. Olague, B. Lu, J. Wilson, and F. Khalife for their help with data collection.

REFERENCES

[1] K. Dogancay
UAV path planning for passive emitter localization
IEEE Trans. Aerosp. Electron. Syst., vol. 48, no. 2, pp. 1150–1166, Apr. 2012.

[2] Z. Kassas and U. Ozguner
A nonlinear filter coupled with hospitability and synthetic inclination maps for in-surveillance and out-of-surveillance tracking
IEEE Trans. Syst., Man, Cybern., Part C, Appl. Rev., vol. 40, no. 1, pp. 87–97, Jan. 2010.

[3] J. Kim and S. Sukkarieh
Autonomous airborne navigation in unknown terrain environments
IEEE Trans. Aerosp. Electron. Syst., vol. 40, no. 3, pp. 1031–1045, Jul. 2004.

[4] Y. Oshman
Optimal sensor selection strategy for discrete-time state estimators
IEEE Trans. Aerosp. Electron. Syst., vol. 30, no. 2, pp. 307–314, Apr. 1994.

[5] W. Meng, L. Xie, and W. Xiao
Optimal TDOA sensor-pair placement with uncertainty in source location
IEEE Trans. Veh. Technol., vol. 65, no. 11, pp. 9260–9271, Jan. 2016.

[6] H. Zhang
Two-dimensional optimal sensor placement
IEEE Trans. Syst., Man Cybern., vol. 25, no. 5, pp. 781–792, May 1995.

[7] D. Jourdan and N. Roy
Optimal sensor placement for agent localization
In *Proc. IEEE/ION Position, Location, Navig. Symp.*, Apr. 2006, pp. 128–139.

[8] J. Isaacs, D. Klein, and J. Hespanha
Optimal sensor placement for time difference of arrival localization
In *Proc. IEEE Conf. Decis. Control*, Dec. 2009, pp. 7878–7884.

[9] C. Yang, L. Kaplan, E. Blasch, and M. Bakich
Optimal placement of heterogeneous sensors for targets with Gaussian priors
IEEE Trans. Aerosp. Electron. Syst., vol. 49, no. 3, pp. 1637–1653, Jul. 2013.

[10] J. Raquet and R. Martin
Non-GNSS radio frequency navigation
In *Proc. IEEE Int. Conf. Acoust., Speech Signal Process.*, Mar. 2008, pp. 5308–5311.

[11] L. Merry, R. Faragher, and S. Schedin
Comparison of opportunistic signals for localisation
In *Proc. IFAC Symp. Intell. Auton. Veh.*, Sep. 2010, pp. 109–114.

[12] K. Pesyna, Z. Kassas, J. Bhatti, and T. Humphreys
Tightly-coupled opportunistic navigation for deep urban and indoor positioning
In *Proc. Inst. Navigat. GNSS Conf.*, Sep. 2011, pp. 3605–3617.

[13] Z. Kassas
Analysis and synthesis of collaborative opportunistic navigation systems
Ph.D. dissertation, University of Texas at Austin, Austin, TX, USA, 2014.

[14] V. Moghtadaiee and A. Dempster
Indoor location fingerprinting using FM radio signals
IEEE Trans. Broadcast., vol. 60, no. 2, pp. 336–346, Jun. 2014.

[15] J. Khalife, K. Shamaei, and Z. Kassas
A software-defined receiver architecture for cellular CDMA-based navigation
In *Proc. IEEE/ION Position, Location, Navig. Symp.*, Apr. 2016, pp. 816–826.

[16] C. Yang, T. Nguyen, and E. Blasch
Mobile positioning via fusion of mixed signals of opportunity
IEEE Aerosp. Electron. Syst. Mag., vol. 29, no. 4, pp. 34–46, Apr. 2014.

[17] P. Thevenon *et al.*
Positioning using mobile TV based on the DVB-SH standard
NAVIGATION, J. Institute Navig., vol. 58, no. 2, pp. 71–90, 2011.

[18] K. Pesyna, Z. Kassas, and T. Humphreys
Constructing a continuous phase time history from TDMA signals for opportunistic navigation
In *Proc. IEEE/ION Position Location Navig. Symp.*, Apr. 2012, pp. 1209–1220.

[19] J. Khalife, Z. Kassas, and S. Saab
Indoor localization based on floor plans and power maps: Non-line of sight to virtual line of sight
In *Proc. Inst. Navigat. GNSS Conf.*, Sep. 2015, pp. 2291–2300.

[20] J. Morales, J. Khalife, and Z. Kassas
GNSS vertical dilution of precision reduction using terrestrial signals of opportunity
In *Proc. Inst. Navigat. Int. Tech. Meeting Conf.*, Jan. 2016, pp. 664–669.

[21] Z. Kassas and T. Humphreys
The price of anarchy in active signal landscape map building
In *Proc. IEEE Global Conf. Signal Inf. Process.*, Dec. 2013, pp. 165–168.

[22] Z. Kassas and T. Humphreys
Observability analysis of collaborative opportunistic navigation with pseudorange measurements
IEEE Trans. Intell. Transp. Syst., vol. 15, no. 1, pp. 260–273, Feb. 2014.

[23] Z. Kassas
Collaborative opportunistic navigation
IEEE Aerosp. Electron. Syst. Mag., vol. 28, no. 6, pp. 38–41, Jun. 2013.

[24] Z. Kassas and T. Humphreys
Motion planning for optimal information gathering in opportunistic navigation systems
In *Proc. AIAA Guid., Navig., Control Conf.*, Aug. 2013, 551–4565.

[25] Z. Kassas, A. Arapostathis, and T. Humphreys
Greedy motion planning for simultaneous signal landscape mapping and receiver localization
IEEE J. Sel. Top. Signal Process., vol. 9, no. 2, pp. 247–258, Mar. 2015.

[26] Z. Kassas and T. Humphreys
Receding horizon trajectory optimization in opportunistic navigation environments
IEEE Trans. Aerosp. Electron. Syst., vol. 51, no. 2, pp. 866–877, Apr. 2015.

[27] P. Massat and K. Rudnick
Geometric formulas for dilution of precision calculations
NAVIGATION, J. Inst. Navig., vol. 37, no. 4, pp. 379–391, 1990.

[28] N. Levanon
Lowest GDOP in 2-D scenarios
IEE Proc. Radar, Sonar Navig., vol. 147, no. 3, pp. 149–155, Jun. 2000.

[29] I. Sharp, K. Yu, and Y. Guo
GDOP analysis for positioning system design
IEEE Trans. Veh. Technol., vol. 58, no. 7, pp. 3371–3382, Sep. 2009.

[30] N. Blanco-Delgado and F. Nunes
Satellite selection method for multi-constellation GNSS using convex geometry
IEEE Trans. Veh. Technol., vol. 59, no. 9, pp. 4289–4297, Nov. 2010.

[31] S. Martinez and F. Bullo
Optimal sensor placement and motion coordination for target tracking
Automatica, vol. 42, no. 4, pp. 661–668, Apr. 2006.

[32] W. Meng, L. Xie, and W. Xiao
Optimality analysis of sensor-source geometries in heterogeneous sensor networks
IEEE Trans. Wireless Commun., vol. 12, no. 4, pp. 1958–1967, Apr. 2013.

[33] J. Spilker, Jr.
Satellite Constellation and Geometric Dilution of Precision
In *Global Positioning System: Theory and Applications*. Washington, DC, USA: American Institute of Aeronautics and Astronautics, 1996, ch. 5, pp. 177–208.

[34] A. Bishop, B. Fidan, B. Anderson, K. Dogancay, and P. Pathirana
Optimality analysis of sensor-target localization geometries
Automatica, vol. 46, pp. 479–492, 2010.

[35] N. Blanco-Delgado , F. Nunes, and G. Seco-Granados
Relation between GDOP and the geometry of the satellite constellation
In *Proc. Int. Conf. Localization GNSS*, Jun. 2011, pp. 175–180.

[36] J. Morales and Z. Kassas
Optimal receiver placement for collaborative mapping of signals of opportunity
In *Proc. Inst. Navigat. GNSS Conf.*, Sep. 2015, pp. 2362–2368.

[37] D. Moreno-Salinas , A. Pascoal, and J. Aranda
Optimal sensor placement for multiple target positioning with range-only measurements in two-dimensional scenarios
Sensors, vol. 13, no. 8, pp. 10674–10710, 2013.

[38] A. Thompson, J. Moran, and G. Swenson
Interferometry and Synthesis in Radio Astronomy, 2nd ed. New York, NY, USA: Wiley, 2001.

[39] Y. Bar-Shalom, X. Li, and T. Kirubarajan
Estimation With Applications to Tracking and Navigation. New York, NY, USA: Wiley, 2002.

[40] D. Uciński
Optimal Measurement Methods for Distributed Parameter System Identification. Boca Raton, FL, USA: CRC Press, 2005.

[41] S. Boyd and L. Vandenberghe
Convex Optimization. Cambridge, U.K: Cambridge Univ. Press, 2004.

[42] A. Engle
Problem-Solving Strategies, 1st ed. New York, NY, USA: Springer, 1998.

[43] R. Graham, D. Knuth, and O. Patashnik
Concrete Mathematics: A Foundation for Computer Science. Reading, MA, USA: Addison-Wesley, 1994.

[44] T. Humphreys, J. Bhatti, T. Pany, B. Ledvina, and B. O'Hanlon
Exploiting multicore technology in software-defined GNSS receivers
In *Proc. Inst. Navigat. GNSS Conf.*, Sep. 2009, pp. 326–338.

[45] R. Roy and T. Kailath
ESPRIT-estimation of signal parameters via rotational invariance techniques
IEEE Trans. Acoust., Speech, Signal Process., vol. 37, no. 7, pp. 984–995, Jul. 1989.

[46] B. Fleury, M. Tschudin, R. Heddergott, D. Dahlhaus, and K. Pedersen
Channel parameter estimation in mobile radio environments using the SAGE algorithm
IEEE J. Sel. Areas Commun., vol. 17, no. 3, pp. 434–450, Mar. 1999.

[47] P. Brockwell and R. Davis
Introduction to Time Series and Forecasting, 3rd ed. New York, NY, USA: Springer, 2016.

[48] C. Chatfield
Time-Series Forecasting. Boca Raton, FL, USA: CRC Press, 2000.

[49] C. Ansley, W. Spivey, and W. Wrobleski
On the structure of moving average processes
J. Econometrics, vol. 6, no. 1, pp. 121–134, Jul. 1976.

[50] S. Narla
The evolution of connected vehicle technology: From smart drivers to smart cars to... self-driving cars
Inst. Transp. Eng. J., vol. 83, no. 7, pp. 21–26, 2013.

[51] Z. Kassas, V. Ghadiok, and T. Humphreys
Adaptive estimation of signals of opportunity
In *Proc. Inst. Navigat. GNSS Conf.*, Sep. 2014, pp. 1679–1689.

Joshua J. Morales (S'11) received the B.S. degree (high honors) in electrical engineering from the University of California, Riverside, Riverside, CA, USA, where he is currently working toward the Ph.D. degree in electrical engineering in the Department of Electrical and Computer Engineering.

He is a Member of the Autonomous Systems Perception, Intelligence, and Navigation Laboratory. His research interests include estimation, navigation, autonomous vehicles, and intelligent transportation systems.

Zaher M. Kassas (S'98–M'08–SM'11) received the B.E. degree in electrical engineering from the Lebanese American University, Beirut, Lebanon, the M.S. degree in electrical and computer engineering from the Ohio State University, Columbus, OH, USA, and the M.S.E. degree in aerospace engineering and the Ph.D. in electrical and computer engineering, both from the University of Texas at Austin, Austin, TX, USA.

From 2004 to 2010, he was a Research and Development Engineer in the LabVIEW Control Design and Dynamical Systems Simulation Group at National Instruments Corp. He is currently an Assistant Professor at the University of California, Riverside, CA, USA and the Director of the ASPIN Laboratory, Riverside, CA, USA. His research interests include cyber-physical systems, estimation theory, navigation systems, autonomous vehicles, and intelligent transportation systems.